

Mixed-mode oscillations in coupled FitzHugh-Nagumo oscillators: blow-up analysis of cusped singularities

Kristian Uldall Kristiansen^{*1} and Morten Gram Pedersen²

¹Department of Applied Mathematics and Computer Science,
Technical University of Denmark, 2800 Kgs. Lyngby, Denmark

²Department of Information Engineering, University of Padova, 35131
Padova, Italy

November 18, 2022

Abstract

In this paper, we use geometric singular perturbation theory and blowup, as our main technical tool, to study the mixed-mode oscillations (MMOs) that occur in two coupled FitzHugh-Nagumo units with symmetric and repulsive coupling. In particular, we demonstrate that the MMOs in this model are not due to generic folded singularities, but rather due to singularities at a cusp – not a fold – of the critical manifold. Using blowup, we determine the number of SAOs analytically, showing – as for the folded nodes – that they are determined by the Weber equation and the ratio of eigenvalues. We also show that the model undergoes a (symmetric) saddle-node bifurcation in the desingularized reduced problem, which – although resembling a folded saddle-node (type II) at this level – also occurs on a cusp, and not a fold. We demonstrate that this bifurcation is associated with the emergence of an invariant cylinder, the onset of SAOs, as well as SAOs of increasing amplitude. We relate our findings with numerical computations and find excellent agreement.

Keywords Mixed-mode oscillations, cusp, folded singularities, canards, blowup, geometric singular perturbation theory.

MSC 34C15, 34D15, 37E17

^{*}Corresponding author, krkri@dtu.dk

1 Introduction

Coupled nonlinear oscillators are ubiquitous in physics, chemistry, biology and many other contexts. Interestingly, the collective behavior of the population of oscillators may exhibit qualitatively different dynamics than the individual units would if uncoupled. Coupling may, e.g., lead to oscillator death [2, 14] or, on the contrary, promote oscillatory activity [17, 51, 52]. In neurons and other cells capable of exhibiting complex bursting electrical activity, gap junction coupling can change the cellular behavior from a simple action potential firing to bursting [10, 33, 38, 44, 45] and lead to large increases in the burst period [34].

A particular kind of complex dynamics, also observed in models of cellular electrical activity, consist of mixed-mode oscillations (MMOs) where small- and large-amplitude oscillations (SAOs and LAOs, respectively) alternate [6, 11]. Such dynamics is caused by cellular mechanisms operating on different time scales and can be seen, e.g., in the classical Hodgkin-Huxley model [22] for neuronal action potential generation [43], and in experimental data and models of cortical neurons [20], stellate cells [12, 42], neuroendocrine cells [3, 41, 48, 49], cardiac cells [26, 54], among others. The mathematical structure causing MMOs is increasingly well understood by Geometric Singular Perturbation Theory (GSPT henceforth) [15, 25] and often involves folded singularities, canard orbits [46, 53] and singular Hopf bifurcations [18], which are generally related to saddle-node bifurcations in the fast subsystem when treating slow variables as parameters [6, 11].

In our recent study of coupled bursting oscillators [39], we revisited the finding by Sherman [44] who showed that coupling of spiking cells can lead to bursting via slow desynchronization so that each burst is preceded by a large number of full action potentials (spikes). Before the transition to bursting, the averaged membrane potentials show SAOs reflecting amplitude-modulated spiking [39]. We showed that the dynamical structure of the system obtained by averaging was captured by a system of two coupled FitzHugh-Nagumo (FHN) units [16, 35]:

$$\begin{aligned}\dot{v}_1 &= -v_1^3 + 3v_1 - w_1 + g(v_2 - v_1), \\ \dot{v}_2 &= -v_2^3 + 3v_2 - w_2 + g(v_1 - v_2), \\ \dot{w}_1 &= \epsilon(v_1 - c), \\ \dot{w}_2 &= \epsilon(v_2 - c),\end{aligned}\tag{1}$$

with symmetric and repulsive coupling $g < 0$, and that this simple system exhibits MMOs organized by a singular Hopf bifurcation related to a folded singularity [18]. However, this bifurcation was not related to a transcritical bifurcation of a folded node (the folded saddle-node [31]), as is typically seen in applications [11], but rather to a cusp catastrophe in the fast subsystem. This observation motivated the current study of what we will refer to as

cusped singularities.

1.1 Background

In this paper, we continue our study of the two identical FHN units (1). We start by highlighting three separate properties. Firstly, for $g = 0$ then (v_1, w_1) and (v_2, w_2) decouple as a Lienard equation:

$$\begin{aligned}\dot{v}_i &= -v_i^3 + 3v_i - w_i, \\ \dot{w}_i &= \epsilon(v_i - c),\end{aligned}\tag{2}$$

for $i = 1, 2$, and the dynamics of each pair is identical, being oscillatory (through relaxation oscillations) for $c \in (-1, 1)$ and nonoscillatory (through a globally attracting equilibrium) for $c > 1$ (and $c < -1$) for all $0 < \epsilon \ll 1$ [16, 23], see Fig. 1.

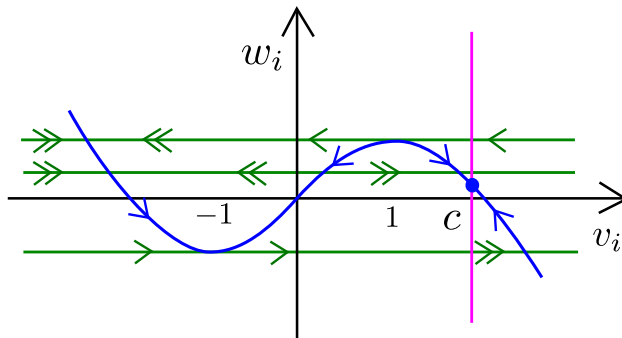


Figure 1: Slow-fast dynamics of (1) in the uncoupled case $g = 0$. The blue curve is the (cubic) critical manifold, whereas the vertical purple line is the w_i -nullcline. The case illustrated is for $c > 1$ where there is an attracting equilibrium of the reduced problem on the rightmost stable branch of the critical manifold. For $c = 1$ there is a canard point at the right most fold, leading to stable relaxation oscillations for $c \in (-1, 1)$ and all $0 < \epsilon \ll 1$.

Secondly, the system (1) is symmetric with respect to

$$\mathcal{S} : (v_1, v_2, w_1, w_2) \mapsto (v_2, v_1, w_2, w_1),$$

so that $v_1 = v_2$, $w_1 = w_2$, being the fixed point of this symmetry, defines an invariant subspace. This will play an important role in the following.

Finally, there is a unique equilibrium

$$q : (v_1, v_2, w_1, w_2) = (c, c, -c^3 + 3c, -c^3 + 3c),\tag{3}$$

of (1) and this point q lies on the symmetric subspace defined by $v_1 = v_2$,

$w_1 = w_2$. The Jacobian evaluated at q has eigenvalues

$$\nu_{1,2} = \frac{3 - 3c^2 \pm \sqrt{(3 - 3c^2)^2 - 4\epsilon}}{2}, \quad (4)$$

$$\nu_{3,4} = \frac{3 - 3c^2 - 2g \pm \sqrt{(3 - 3c^2 - 2g)^2 - 4\epsilon}}{2}. \quad (5)$$

Let

$$v_s(g) := \sqrt{1 - \frac{2}{3}g}. \quad (6)$$

Then a Hopf bifurcation occurs for $c = v_s(g)$ where $\nu_{3,4}$ are purely imaginary ($\pm i\sqrt{\epsilon}$). In fact, a direct calculation (based upon center manifold and normal form theory, see specifically [19, Equation 3.4.11] and Remark 6 below) shows that the associated first Liapunov number is given by

$$l_1(\epsilon) = \frac{3(g - 3)}{8g\sqrt{\epsilon}}(1 + \mathcal{O}(\epsilon)). \quad (7)$$

Seeing that $l_1(\epsilon) > 0$ for $g < 0$ and all $0 < \epsilon \ll 1$, it follows that we have a (singular) subcritical Hopf bifurcation [18, 19] for all $\epsilon > 0$ small enough.

In [39], it was observed numerically that the system (1) for $c < v_s$ but $c \approx v_s$ and $0 < \epsilon \ll 1$ exhibits mixed-mode oscillations (MMOs) with an increasing number of small-amplitude oscillations (SAOs) as c approaches v_s from below, see Fig. 2, Fig. 3, Fig. 4 and the figure captions. Following large-amplitude oscillations (LAOs), the two cells almost synchronize ($v_1 \approx v_2$). However, as the voltages approach c , they begin to diverge as they spiral apart, creating SAOs with increasing amplitudes before departing into additional large-amplitude excursions. Interestingly, for some c values, e.g., $c = 1.27$, there is an alternation between v_1 and v_2 being increasing (and v_2 , respectively, v_1 being decreasing) at the beginning of the LAOs, whereas this does not occur for other c values. We will show that this phenomenon corresponds to the system leaving the neighborhood of the cusped singularity in different directions, a behavior which is not possible for the standard folded node. We return to this point in the Conclusions.

1.2 Biophysical motivation and implications

Since the FHN model is a simplification of the Hodgkin-Huxley model for neuronal activity, our results have implication for neuroscience beyond providing insight into our previous study [39]. Negative coupling ($g < 0$) resembles mutual inhibition, for example between neuronal populations, see e.g. Curtu and Rubin [8, 9]. These authors showed that MMOs can appear as a result of inhibition via a singular Hopf bifurcation. Mutual inhibition has also been used to explain “binocular rivalry”, where perception alternates between different images presented to each eye [32].

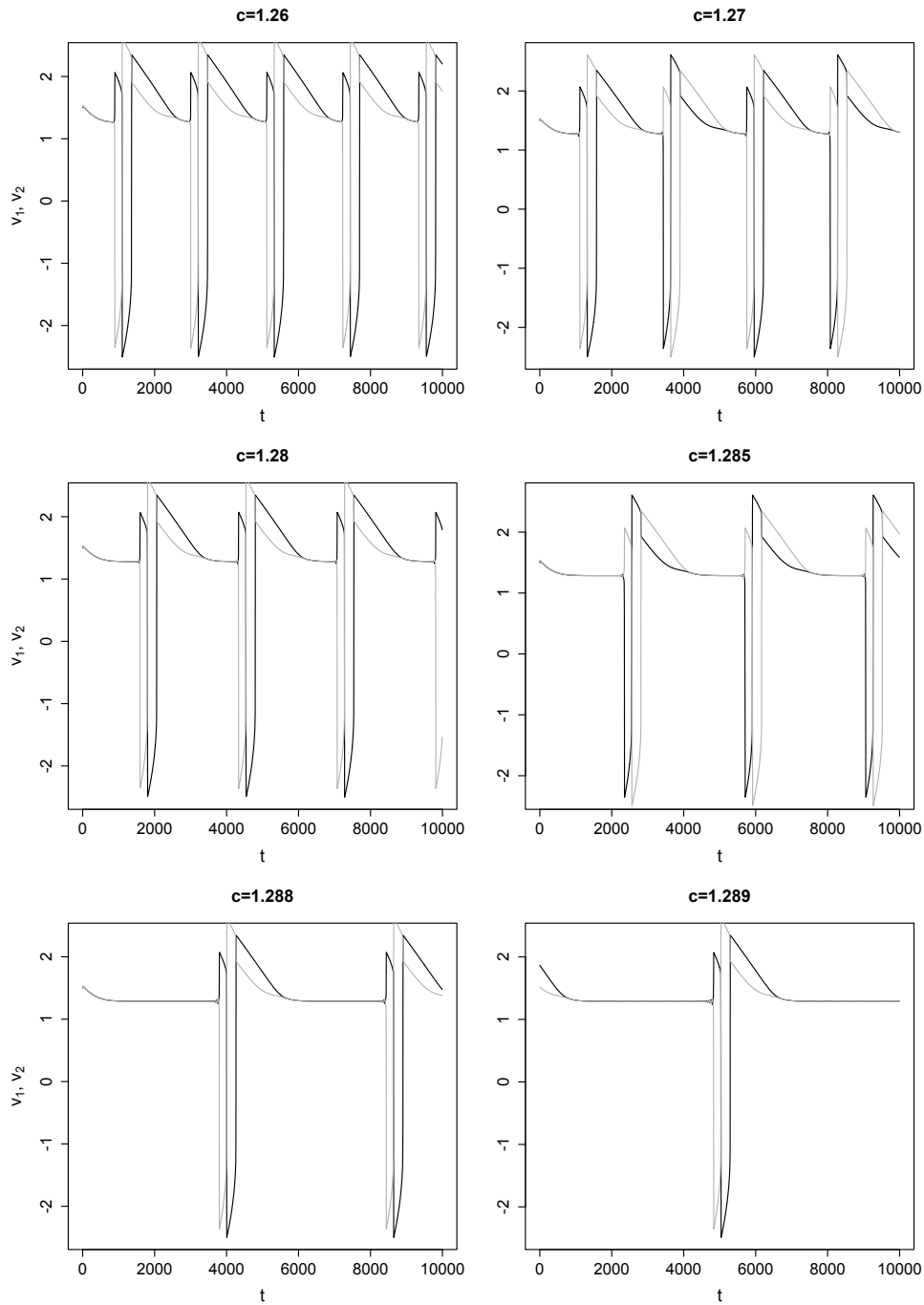


Figure 2: MMOs for $g = -1$, $\epsilon = 0.01$ and c values as indicated. Black and gray curves show, respectively, $v_1(t)$ and $v_2(t)$. For a zoom on the SAOs, see Fig. 3.

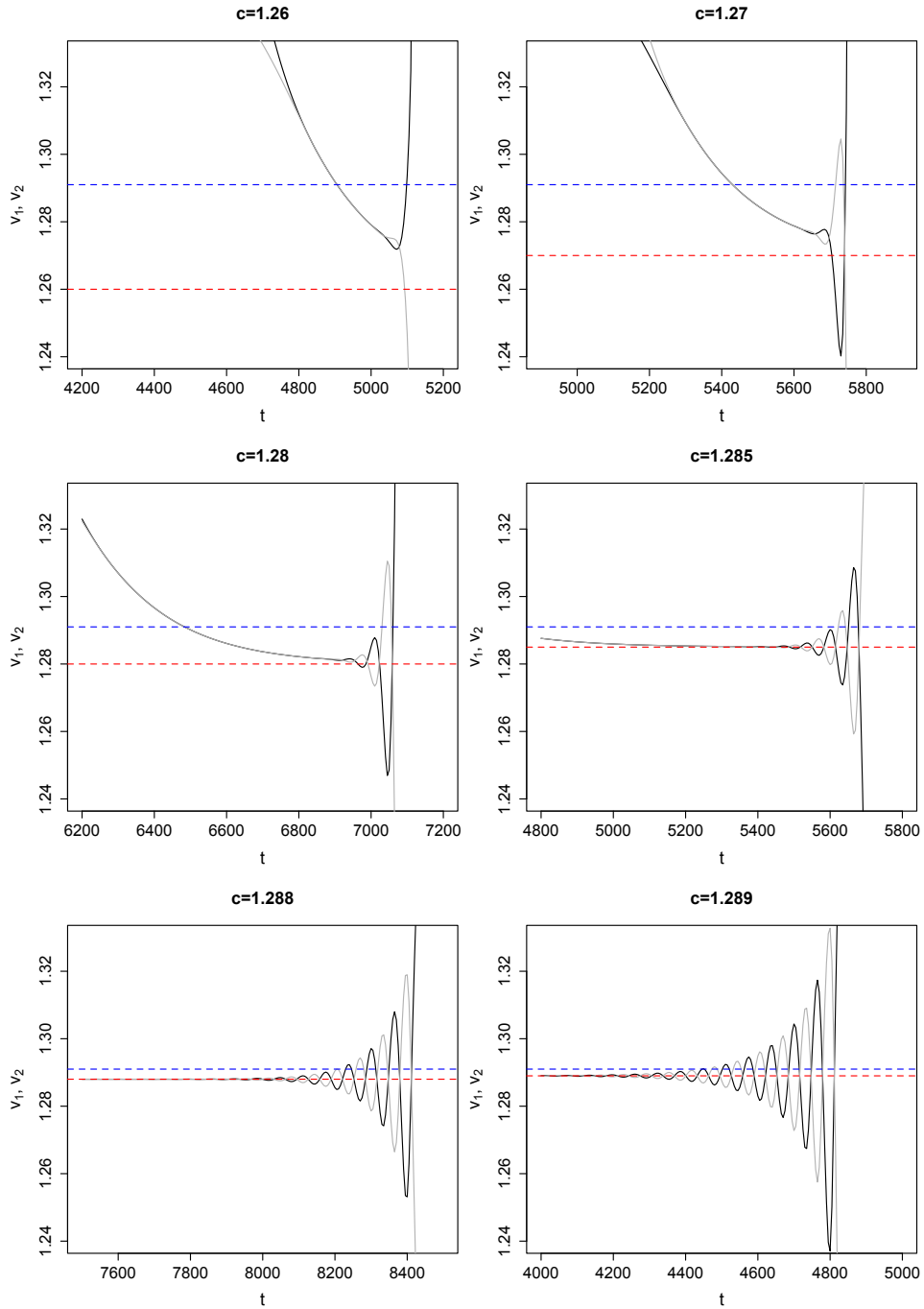


Figure 3: Zoom on the SAOs in Fig. 2 near $v_s = \sqrt{5/3} \approx 1.291$ (blue dashed line) with c values (red dashed) as indicated. Note how the number of SAOs increases as c approaches v_s .

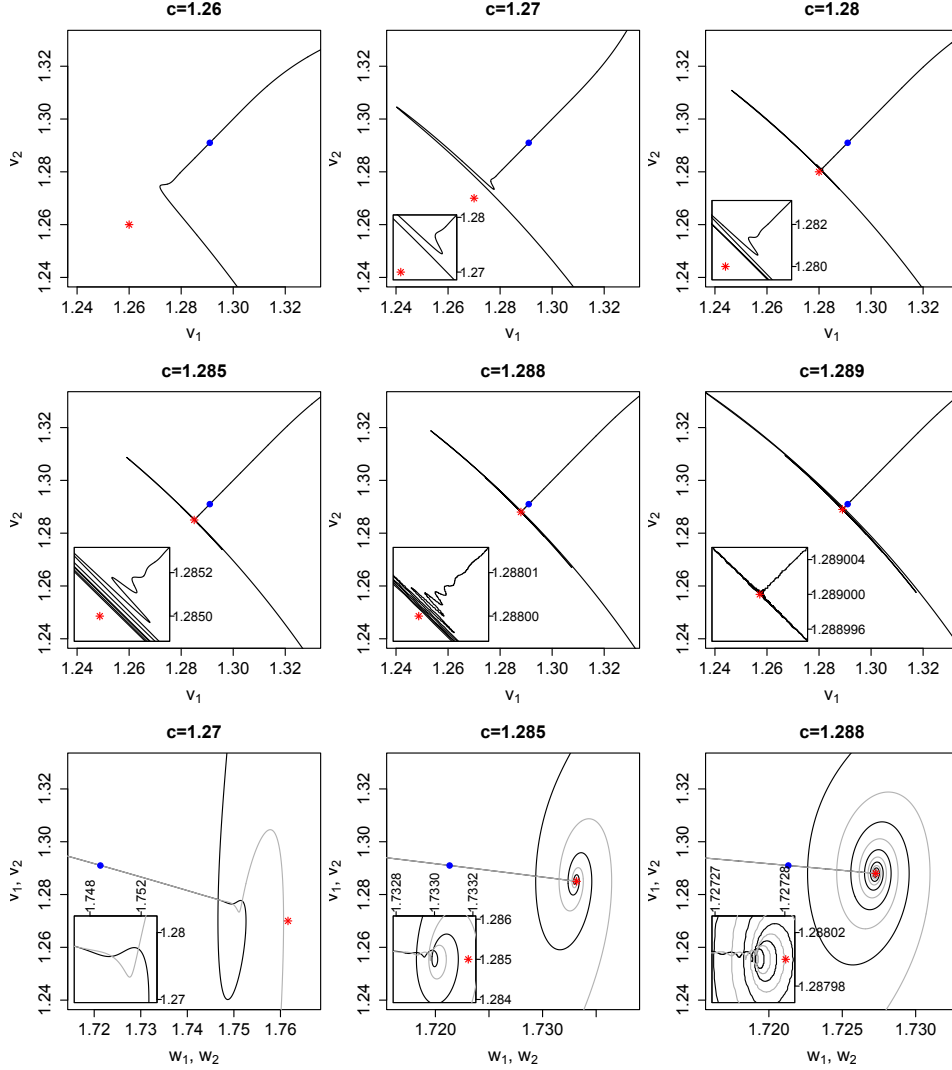


Figure 4: SAOs near the folded singularity $(v_1, v_2, w_1, w_2) = (v_s, v_s, w_s, w_s)$ where $w_s = -v_s^3 + 3v_s$ (blue dot; see Proposition 1). The full-system saddle point (3) is shown as a red asterisk. In the lower panels, the black and gray curves show, respectively, (w_1, v_1) and (w_2, v_2) . Insets show zooms on the SAOs near the saddle point. Parameters as in Fig. 2.

As explained above, our choice of $c > 1$ (similarly, one could consider $c < -1$) means that the FHN neurons are silent when uncoupled. Our results show that repulsive coupling can induce oscillatory activity in such otherwise silent neurons via MMOs related to cusped singularities. These results mimic previous findings for “release” and “escape” mechanisms generating oscillations in a couple of inhibitory non-oscillatory neurons [51]. We

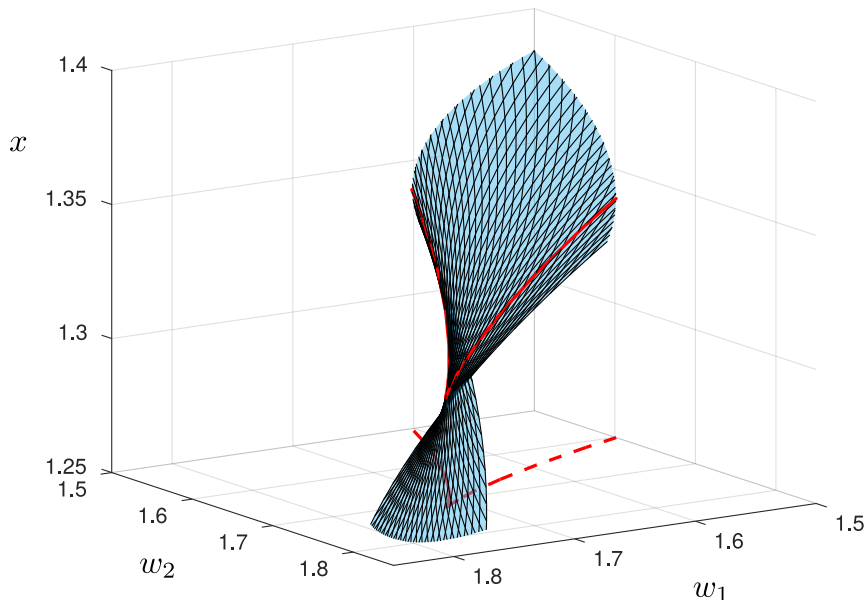


Figure 5: The two-dimensional critical manifold C of (1) viewed in the (w_1, w_2, x) -space with $x = \frac{1}{2}(v_1 + v_2)$ for $g = -1$. The red curve is a set of non-normally hyperbolic points. The projection onto the (w_1, w_2) -plane shows the cusp singularity. (1) has a cusped node (cusped saddle-node) for $c \approx v_s$ but $c < v_s$ ($c = v_s$, respectively), insofar that the reduced problem has a folded singularity on the cusp of nodal type (saddle-node type, respectively) upon desingularization.

do not consider $-1 < c < 1$ or $g > 0$ since the system in these cases does not present a cusped singularity producing SAOs, which is the main topic of the manuscript.

1.3 Main results

In this paper, we describe the origin and mechanisms underlying the MMOs in Fig. 2, Fig. 3 and Fig. 4. In particular, we show that the coupled system (1) possesses a degenerate folded singularity in the singular limit $\epsilon \rightarrow 0$, and demonstrate – through a center manifold computation – that this singularity corresponds to a cusp, see also Fig. 5 and the figure caption for details. Moreover, by performing a detailed blow-up analysis, we dissect the details of the dynamics near this new type of singularity and show that it lies at the heart of the mechanism causing SAOs. As for folded singularities [46], we divide our analysis into two parts: one part covering the generic case (i.e. without an additional unfolding parameter) and one covering the bifurcation

in the presence of an unfolding parameter. Since, the former case resembles the folded node [53] – in particular, we will show that the number of SAOs is also determined by the Weber equation and the ratio of eigenvalues – we will refer to this singularity as the “cusped node singularity”. Similarly, our results also show that the degenerate case, which we name the “cusped saddle-node singularity”, as the classical folded saddle-node (of type II [31]), marks the onset of SAOs in the coupled FHN system.

For any $b \geq 0$, let $\lfloor b \rfloor$, denote the largest integer $n \in \mathbb{N}_0$ such that $n \leq b$. We then summarize our findings on the SAOs in the following theorem (we refer to Theorem 2 and Theorem 3 for more detailed versions).

Theorem 1 *Consider (1) with $g < 0$ and suppose*

$$c \in \left(\frac{1 - \frac{1}{2}g}{\sqrt{1 - \frac{2g}{3}}}, v_s \right). \quad (8)$$

Then we have (the cusped-node case):

1. *There is a desingularization of the reduced problem on the critical manifold C of the slow-fast system (1) such that the system has an attracting singularity f_1 , given by*

$$v_i = v_s, \quad w_i = w_s, \quad \text{for } i = 1, 2,$$

for $w_s := -v_s^3 + 3v_s$, that lies on a cusp of C . Moreover, the linearization around f_1 has the following eigenvalues

$$\lambda_1 := -6v_s(v_s - c), \quad \lambda_2 := -\lambda_1 + 2g. \quad (9)$$

with $\lambda_2 < \lambda_1 < 0$ for the values in (8). The point f_1 is therefore a stable node for the desingularized system; specifically, it (locally) attracts all points on the attracting subset of C .

2. *Orbits of (1) that pass through f_1 for $0 < \epsilon \ll 1$ will (in general) undergo SAOs around the symmetric subspace $v_1 = v_2$, $w_1 = w_2$ before leaving a neighborhood of f_1 .*
3. *Suppose that $\frac{\lambda_2}{\lambda_1} \notin \mathbb{N}$. Then the amplitude of these SAOs is of the order $\mathcal{O}(\epsilon^{\frac{\lambda_2}{2\lambda_1}})$ and the number of SAOs is given by $\lfloor \frac{\lambda_2}{\lambda_1} \rfloor$ many full 180° rotations around the symmetric subspace $v_1 = v_2$, $w_1 = w_2$, for all $0 < \epsilon \ll 1$.*

Next, fix any

$$c_2 \in \left(-\frac{1}{3v_s}, 0 \right), \quad (10)$$

and consider

$$c = v_s + \sqrt{\epsilon}c_2. \quad (11)$$

Then we have (the cusped-saddle node case):

4. The singularity f_1 of the desingularized reduced problem on C is a saddle-node for $c = v_s$ with $\lambda_2 < \lambda_1 = 0$, locally attracting all points on the attracting subset of C .
5. With c as in (11) and c_2 fixed in (10), the regular singularity q , given by (3), is of saddle-focus type for all $0 < \epsilon \ll 1$, having a two-dimensional unstable manifold with focus-type dynamics.
6. Orbits of (1), with c as in (11) and c_2 fixed in (10), that pass through f_1 for $0 < \epsilon \ll 1$ will (in general) undergo SAOs around the symmetric subspace $v_1 = v_2$, $w_1 = w_2$, before leaving a neighborhood of f_1 .
7. There are finitely many of the SAOs that are $\mathcal{O}(\epsilon^{1/4})$ in amplitude as $\epsilon \rightarrow 0$.
8. The number of SAOs with an amplitude that is exponentially small with respect to $\epsilon > 0$ is unbounded as $\epsilon \rightarrow 0$.

There are no SAOs for $c_2 > 0$ and all $0 < \epsilon \ll 1$. □

Despite the similarities between the folded and cusped versions of the singularities, we will also illuminate some differences. For example, we show that the cusped saddle-node is intrinsically related to a regular Liénard equation in the same way that the FSN is related to the canard explosion. See Lemma 9 and Proposition 6 for details.

Remark 1 The reference [29] also considers coupled oscillators in four dimensions, including systems like (1). The focus is (also) on emergence of MMOs in these types of systems. However, in contrast to our work, the singularities in [29] are folded and not “cusped” and the analysis of the coupled FitzHugh-Nagumo system, see [29, Section 4], also focuses on the attractive coupling $g > 0$. In the present paper, we will only consider $g < 0$.

1.4 Numerical results

To illustrate Theorem 1, we compare the theoretical results to numerical simulations. We define

$$u = \frac{1}{2}(v_1 - v_2), \quad y = \frac{1}{2}(w_1 + w_2) - w_s, \quad z = \frac{1}{2}(w_1 - w_2). \quad (12)$$

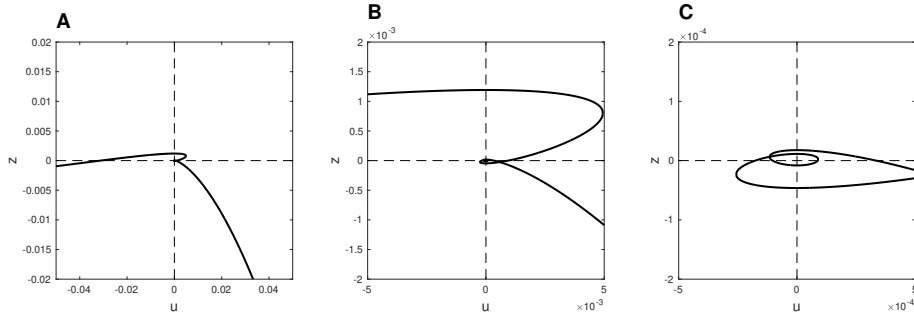


Figure 6: Simulated trajectory projected onto the (u, z) -plane for $c = 1.24$ and $g = -1$ (the cusped node case). Here $\frac{\lambda_2}{\lambda_1} = 4.06$. Panels B and C show zooms on the SAOs near the origin. In agreement with Theorem 1, there are four full 180° -rotations (twists), corresponding to five simple zeros of u , for this value of c . Only three of the twists are visible in the zoom C, the fourth, larger one can be seen in panel B.

In Theorem 1, we count the number of SAOs as 180° -rotations around the symmetric subspace. In the coordinates (12), the symmetric space corresponds to $u = 0, z = 0$, so when projected onto the (u, z) -plane, SAOs correspond to full 180° rotations around the origin. Therefore we have the following: *The number of SAOs is one less than the number of zeros of $u = 0$.* We illustrate this in Fig. 6 for $c = 1.24, g = -1$ and $\epsilon = 0.01$. Here $\frac{\lambda_2}{\lambda_1} = 4.06$ and we find five simple zeros of u and in agreement with Theorem 1 precisely four full 180° -rotations.

On the other hand, Fig. 7A shows a typical orbit of the system (1) in the (u, y, z) -space for $c = 1.28, g = -1, \epsilon = 0.01$. It corresponds to the cusped saddle-node case. The orbit approaches the symmetric subspace $u = 0, z = 0$ denoted by γ (red dotted line), and moves towards and beyond the cusped singularity f_1 located at the origin (blue dot), coming close to the saddle-focus point q (red asterisk) before spiralling outwards. To find the number of SAOs as a function of c , we counted the number of zeros of $u = 0$ as asymptotes of z/u (see Fig. 7B) for a range of c values. These numerical results were then plotted against the theoretical values of item 3 in Theorem 1 using the explicit expressions for the eigenvalues (9), see Fig. 7C. The correspondence is excellent with minor discrepancies for c values in the interval given by (10)-(11), the cusped-saddle node region, where Theorem 1 predicts an unbounded number of exponentially small SAOs as $\epsilon \rightarrow 0$ (see Theorem 1, item 8). This is not a surprise, as Theorem 1, item 3, assumes that c is uniformly bounded away from v_s . The increment in amplitude of the SAOs as c increases and enters the cusped-saddle node region, due to focus dynamics near q , see Theorem 1, items 5 and 6, is also confirmed by the simulations (Fig. 7D).

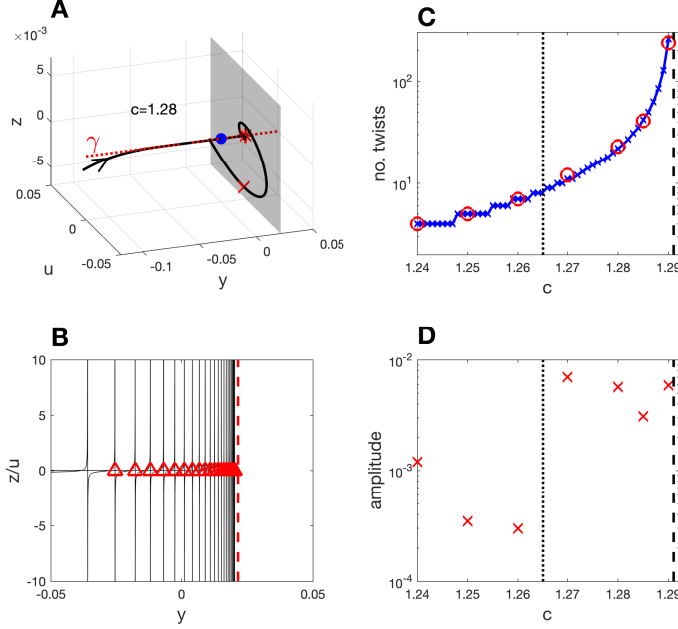


Figure 7: **A**: Simulated trajectory (black curve) in (y, u, z) -space, see (12), with parameters as in Fig. 2 and $c = 1.28$. The blue point is the cusped singularity f_1 . The red asterisk is the full-system saddle-focus point q , which lies in the gray plane given by $y = -c^3 + 3c - w_s$. The red cross indicates the point used to find the amplitude of the z -value at the last twist, cf. panel D. The red dotted line is γ ($u = z = 0$). **B**: Simulation as in panel A but showing z/u as function of y in order to count the number of twists around γ , see Theorem 1, item 2. The red triangles show the asymptotes (where $u = 0$), which were found automatically. The number of SAOs is one less than the number of asymptotes (see the text for further details), which is why the first asymptote is not indicated. The vertical red dashed line indicates the y -value of the saddle-focus. **C**: Number of SAOs predicted from Theorem 1, item 3 (blue crosses), for a series of c values compared to the number of SAOs found from the simulations (red circles), as indicated by the triangles in panel B. The vertical dotted line at $c = v_s - \frac{\sqrt{\epsilon}}{3v_s} \approx 1.265$ indicates the left boundary of the cusped-saddle node case, see Theorem 1, whereas the dashed line is $c = v_s$. **D**: The amplitude of the last rotation (red crosses), estimated as the absolute value of z at the last relevant asymptote, i.e., the right-most triangle in panel B, see the red cross in panel A. The vertical lines are as in panel C. Note how the amplitude increases dramatically as c approaches v_s and enters the saddle-node region with $\mathcal{O}(\epsilon^{1/4})$ -amplitude SAOs.

1.5 Overview

In Section 2, we first study (1) as a singular perturbation problem for $\epsilon \rightarrow 0$ using GSPT. Specifically, we present a complete analysis of the reduced problem for any fixed $g < 0$ and describe all bifurcations for $c > 0$ at the singular level. This then leads to a local three-dimensional center manifold reduction (with parameters ϵ, c and g) in Proposition 2. In Lemma 3, we then show that the critical manifold of this reduced system has a cusp singularity. In Sections 3 and 4, we proceed to study the dynamics near the cusped node and the cusped saddle-node singularity, respectively, by using the blowup method [13, 30] as the main technical tool. This leads to Theorem 2 and Theorem 3 describing the SAOs in the two scenarios. The two theorems imply Theorem 1. In Section 5, we conclude the paper.

2 GSPT-analysis of (1)

To analyze (1) as a slow-fast system, we first study the layer problem and the reduced problem. The layer problem is obtained by setting $\epsilon = 0$ in (1):

$$\begin{aligned} \dot{v}_1 &= -v_1^3 + 3v_1 - w_1 + g(v_2 - v_1), \\ \dot{v}_2 &= -v_2^3 + 3v_2 - w_2 + g(v_1 - v_2), \\ \dot{w}_i &= 0, \end{aligned} \tag{13}$$

for $i = 1, 2$. On the other hand, the reduced problem, given by:

$$\begin{aligned} 0 &= -v_1^3 + 3v_1 - w_1 + g(v_2 - v_1), \\ 0 &= -v_2^3 + 3v_2 - w_2 + g(v_1 - v_2), \\ w_1' &= v_1 - c, \\ w_2' &= v_2 - c, \end{aligned} \tag{14}$$

is obtained by setting $\epsilon = 0$ in the slow time ($\tau = \epsilon t$) version of (1):

$$\begin{aligned} \epsilon v_1' &= -v_1^3 + 3v_1 - w_1 + g(v_2 - v_1), \\ \epsilon v_2' &= -v_2^3 + 3v_2 - w_2 + g(v_1 - v_2), \\ w_1' &= v_1 - c, \\ w_2' &= v_2 - c, \end{aligned}$$

where $()' = d/d\tau$. In the following, we will analyze (13) and (14) successively.

2.1 Analysis of the layer problem (13)

The equilibria of the layer problem are given by

$$\begin{aligned} 0 &= -v_1^3 + 3v_1 - w_1 + g(v_2 - v_1), \\ 0 &= -v_2^3 + 3v_2 - w_2 + g(v_1 - v_2). \end{aligned}$$

This defines a two-dimensional critical manifold C of (13) in the four-dimensional phase space. The manifold C can be written as a graph $w = h(v)$ over v where $h = (h_1, h_2)$ with

$$\begin{aligned} h_1(v_1, v_2) &:= -v_1^3 + 3v_1 + g(v_2 - v_1), \\ h_2(v_1, v_2) &:= -v_2^3 + 3v_2 + g(v_1 - v_2). \end{aligned}$$

We determine the stability of C by linearizing the layer problem (13) around any point $(v, h(v)) \in C$. It is a basic fact, that the nontrivial eigenvalues are given by the eigenvalues of the Jacobian

$$Dh(v_1, v_2) = \begin{pmatrix} -3v_1^2 - g + 3 & g \\ g & -3v_2^2 - g + 3 \end{pmatrix}.$$

The matrix is symmetric, so the eigenvalues are real. Moreover, we have

$$\begin{aligned} \operatorname{tr} Dh &= -3(v_1^2 + v_2^2) + 6 - 2g, \\ \det Dh &= 9v_1^2v_2^2 - 3(3 - g)(v_1^2 + v_2^2) + 3(3 - 2g). \end{aligned}$$

Consequently, $\operatorname{tr} Dh = 0$ defines a circle centered at $(0, 0)$ with radius $\sqrt{2 - \frac{2}{3}g}$. On the other hand, $\det Dh = 0$ can be written in the polar coordinates (r, θ) : $v_1 = r \cos \theta$, $v_2 = r \sin \theta$ as

$$\cos^2(\theta) \sin^2(\theta) r^4 - (1 - \frac{1}{3}g)r^2 + 1 - 2/3g = 0, \quad (15)$$

which is a quadratic equation in r^2 .

Lemma 1 *Consider (15) as an equation for $r > 0$ and suppose that $g < 0$. Then for each $\theta \neq n\pi/2$, $n \in \mathbb{Z}$, there exists two solutions $r = m_u(\theta)$ and $r = m_s(\theta)$ with*

$$0 < m_u(\theta) < \sqrt{2 - \frac{2}{3}g} < m_s(\theta), \quad (16)$$

where

$$m_u : \mathbb{R} \rightarrow \mathbb{R}_+, \quad m_s : \mathbb{R} \setminus \{\theta \neq n\pi/2, n \in \mathbb{Z}\} \rightarrow \mathbb{R}_+,$$

are smooth functions. For $\theta = n\pi/2$, $n \in \mathbb{Z}$, there is only one solution and it is given by $r = m_u(\theta)$. Finally, for each $n \in \mathbb{Z}$:

$$m_s(\pi/4 + n\pi/2) = \min m_s = v_s, \quad m_s(\theta) \rightarrow \infty \quad \text{for } \theta \rightarrow n\pi/2. \quad \square$$

PROOF Follows from a direct calculation. In particular, $\theta = n\pi/2$, $n \in \mathbb{Z}$ are the values where the coefficient of r^4 vanishes. In order to obtain (16), we use that the curves defined by $\operatorname{tr} Dh = 0$ (a circle with radius $r = \sqrt{2 - \frac{2}{3}g}$) and $\det Dh = 0$ do not intersect. To see this, one can use that

$$\operatorname{tr} (Dh)^2 - 4\det Dh = 9(v_1^2 - v_2^2)^2 + 4g^2 > 0.$$

The expressions for $m_{u,s}$ are not important and therefore left out. Following this lemma, we now define C_{RN} , C_{AN} and C_S as the subsets of C with $0 \leq r < m_u(\theta)$, $r > m_s(\theta)$ and $m_u(\theta) < r < m_s(\theta)$, respectively, in the polar coordinates (r, θ) . Let also F_i be the subset of C defined by $r = m_i(\theta)$, $i = u, s$. Then

$$C = C_{RN} \cup F_u \cup C_S \cup F_s \cup C_{AN}.$$

We then conclude the following (see Fig. 8 for an illustration):

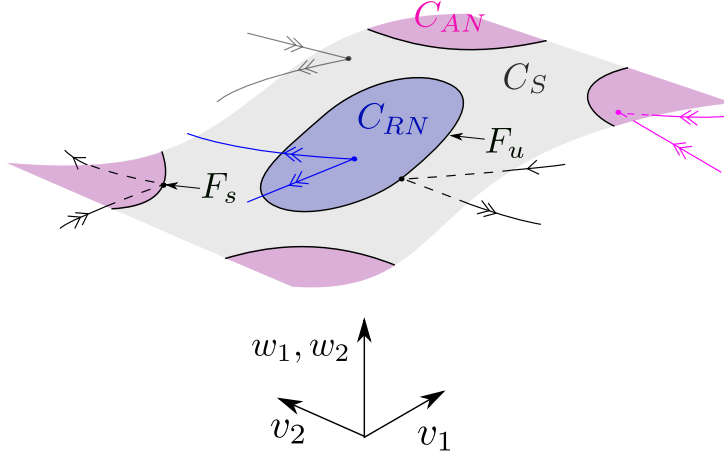


Figure 8: Sketch of the critical manifold. The five sets of curves that are attached to different points on C are orbits of the layer problem (contained within $w_i = \text{const.}$) and indicate the normal stability properties of C along its different components: C_{RN} (repelling, nodal-type), C_S (saddle-type), C_{AN} (attracting, nodal type), F_s and F_u (both saddle-nodes). Here we follow the standard convention that double-headed arrows indicate hyperbolic directions whereas single-headed arrows indicate center/slow directions.

Lemma 2 F_i , $i = u, s$ are sets of loss of normal hyperbolicity, but (since $\text{tr } Dh \geq 0$ on F_i) the linearization along F_u has one positive eigenvalue whereas the nontrivial eigenvalue of the linearization along F_s is negative. Moreover, we have the following classification.

- Suppose $(v, h(v)) \in C_{RN}$. Then the eigenvalues of $Dh(v)$ are both positive and real and v is therefore a repelling node for the fast subsystem of (13).
- Suppose $(v, h(v)) \in C_{AN}$. Then the eigenvalues of $Dh(v)$ are both negative and real and v is therefore an attracting node for the fast subsystem of (13).

- Suppose $(v, h(v)) \in C_S$. Then the eigenvalues of $Dh(v)$ are real and have opposite signs and v is therefore a saddle for the fast subsystem of (13).

In particular, on C_{RN} and C_{AN} , $\det Dh > 0$ whereas $\det Dh < 0$ on C_S . \square

2.2 Analysis of the reduced problem (14)

The reduced problem (14) is defined on C . Since C is a graph over v , we will write this system in terms of v instead of w . This gives

$$Dhv' = v - \mathbf{c}, \quad (17)$$

with

$$\mathbf{c} := (c, c), \quad (18)$$

a notation we adopt in the following. Using the adjugate matrix

$$\text{adj } Dh(v) = \begin{pmatrix} -3v_2^2 - g + 3 & -g \\ -g & -3v_1^2 - g + 3 \end{pmatrix},$$

of Dh , we may write this equation in the following equivalent form:

$$\det Dh(v) v' = \text{adj } Dh(v) (v - \mathbf{c}). \quad (19)$$

On $C_{RN} \cup C_{AN}$, where $\det Dh > 0$, recall Lemma 2, we are therefore led to consider the equivalent system

$$\dot{v} = \text{adj } Dh(v) (v - \mathbf{c}). \quad (20)$$

Since $\det Dh < 0$ on C_S , the *desingularized system* (20) is also equivalent to the reduced problem on C_S upon time reversal. Folded singularities, which organize SAOs and canard trajectories connecting attracting and repelling sheets of the critical manifold, are equilibria of (20) on F_i where $\det Dh = 0$. We then state and prove the following result, see also Fig. 9.

Proposition 1 *Consider (19) with $g < 0$. Then there is a regular singularity $q(c)$ at $v = \mathbf{c}$ for any $c > 0$ and at most four folded singularities:*

1. *There are two folded singularities f_1 and f_2 that exist for all $c > 0$, occur on the symmetric subspace defined by $v_1 = v_2$, and are given by $v = \pm \mathbf{v}_s$ on F_s where*

$$v_s(g) = \sqrt{1 - \frac{2g}{3}}.$$

2. For $c < 1$, then there are two separate folded singularities $f_3(c)$ and $f_4(c)$ that both lie on F_u , but outside the symmetric subspace (i.e $v_1 \neq v_2$ along these), and are given by the equations

$$\begin{aligned} \frac{1}{2}(v_1 + v_2) &= \frac{gc}{3c^2 + g - 3}, \\ \frac{1}{4}(v_1 - v_2)^2 &= \left(\frac{1}{2}(v_1 + v_2) - c \right)^2 + 1 - c^2. \end{aligned} \quad (21)$$

3. For $c > \frac{1-\frac{g}{3}}{\sqrt{1-\frac{2g}{3}}}$, $c \neq \sqrt{1-\frac{g}{3}}$, then $f_3(c)$ and $f_4(c)$ (again given by the equations (21)) are nonsymmetric folded singularities, now located on F_s . $f_3(c)$ and $f_4(c)$ go unbounded as $c \rightarrow \sqrt{1-\frac{g}{3}}$. \square

The point $q(c)$ undergoes two pitchfork bifurcations of (20) at $c = 1$ and $c = \frac{1-\frac{g}{3}}{\sqrt{1-\frac{2g}{3}}}$ (sub and super-critical, respectively, giving rise to $f_3(c)$ and $f_4(c)$ in items 2 and 3), and a transcritical bifurcation at $c = v_s$.

PROOF We use that folded singularities are equilibria of (20) where $v \neq \mathbf{c}$; $v = \mathbf{c}$ corresponds to the regular singularity $q(c)$.

Setting $v_1 = v_2$, we then find the two (isolated) folded singularities f_1 and f_2 given by $v = \pm \mathbf{v}_s$ on F_s , recall (6). When $v_1 \neq v_2$, we consider $u = \frac{1}{2}(v_1 - v_2)$, $x = \frac{1}{2}(v_1 + v_2)$ with $u \neq 0$. This gives

$$x = \frac{gc}{3c^2 + g - 3}, \quad u^2 = (x - c)^2 + 1 - c^2. \quad (22)$$

for $c \neq \sqrt{1-\frac{g}{3}}$. (22) gives (21) upon returning to v_1, v_2 and the existence of $f_3(c)$ and $f_4(c)$. Setting $u = 0$ in (22) gives $c = 1, x = 1$ and $c = \frac{1-\frac{g}{3}}{\sqrt{1-\frac{2g}{3}}}$, $x = v_s$ for $c > 0$. This gives the pitchfork bifurcations. It is a direct calculation to verify the remaining claims regarding $f_3(c)$ and $f_4(c)$ of items 2 and 3. \blacksquare

The linearization of (20) around $v = \mathbf{v}_s(g)$ produces the following eigenvalues:

$$\lambda_1 := -6v_s(v_s - c), \quad \lambda_2 := -\lambda_1 + 2g. \quad (23)$$

It is possible to compute the eigenvalues of the linearization around the other singularities, but they will not be needed. Instead, we just summarize the stability findings of singularities of (20) in Fig. 9. In Fig. 10 we illustrate the reduced problem in the case $\frac{1-\frac{g}{3}}{\sqrt{1-\frac{2g}{3}}} < c < \sqrt{1-\frac{g}{3}}$, where four folded singularities occur and where the regular singularity belongs to C_S and is a saddle for the desingularized reduced problem (20). The case $\sqrt{1-\frac{g}{3}} < c < v_s$ is similar except now the two non-symmetric folded singularities $f_3(c)$ and $f_4(c)$ occur on the F_s -branch located in the lower left corner.

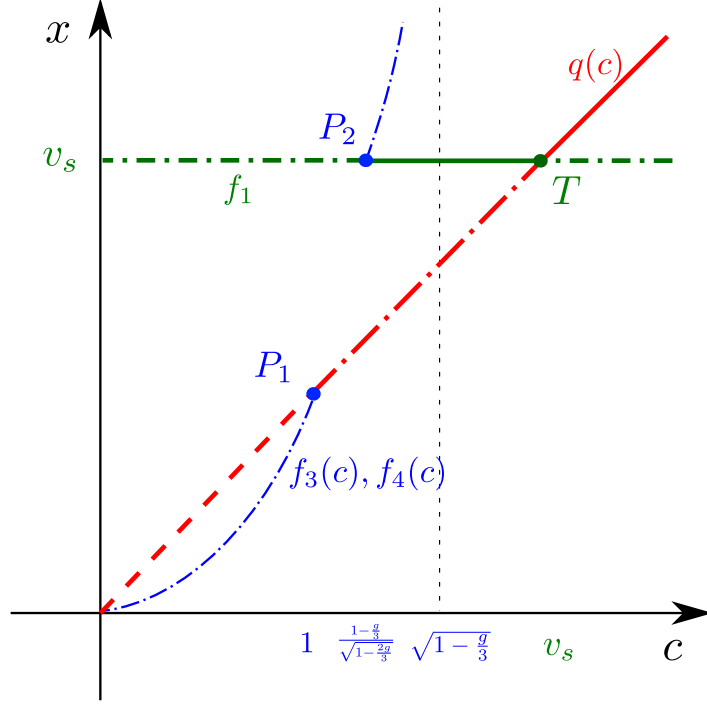


Figure 9: Bifurcation diagram of singularities of (20) using $x = \frac{1}{2}(v_1 + v_2)$ on the vertical axis. Full lines indicate a stable node, dashed-dotted lines a saddle whereas dashed lines indicate an unstable node. In green, we indicate the folded singularity f_1 along $x = v_s$, $u = 0$, whereas the red curve is the regular singularity $q = q(c)$ at $x = c$. The blue curves indicate the pairs $f_3(c)$ and $f_4(c)$ of folded singularities, see Proposition 1 items 2 and 3, that bifurcate from $x = c$ and $x = v_s$ in the pitchfork bifurcations at P_1 and P_2 for $c = 1$ and $c = \frac{1 - \frac{g}{3}}{\sqrt{1 - \frac{2g}{3}}}$, see (22). The value $c = \sqrt{1 - \frac{g}{3}}$ is an asymptote for the pair $f_3(c)$ and $f_4(c)$ of folded singularities in blue. For simplicity, the position of the pair $f_3(c)$ and $f_4(c)$ is not shown for $c > \sqrt{1 - \frac{g}{3}}$. At $c = v_s$ there is a transcritical bifurcation T where the folded singularity at $x = v_s$ exchanges stability with the regular singularity $x = c$.

2.3 Center manifold reduction

We will now perform a center manifold reduction near F_s , which consist of partially hyperbolic points for $\epsilon = 0$, recall Lemma 2. In particular, the reduction will be based upon a local computation near the point $v = \mathbf{v}_s$, $w = \mathbf{w}_s$, where

$$w_s := h_1(\mathbf{v}_s) = -v_s^2 + 3v_s.$$

(Recall the notation (18): $\mathbf{u} = (u, u)$ for any u .) In further details, we consider the extended system ((1), $\dot{\epsilon} = 0$). Then $(v, w, \epsilon) = (\mathbf{v}_s, \mathbf{w}_s, 0)$ is

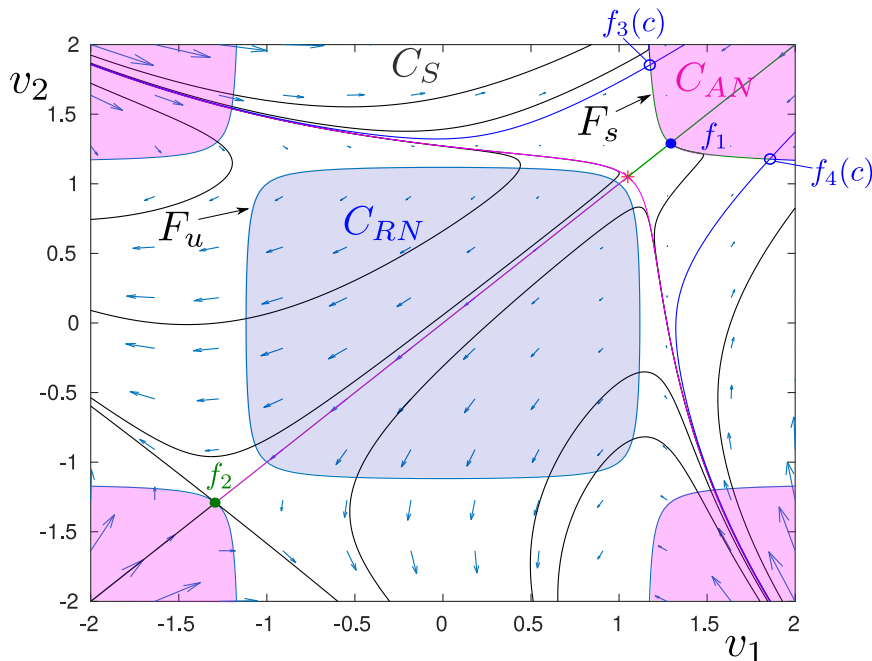


Figure 10: The phase portrait of the desingularized reduced problem (20) in the v -plane for $\frac{1-\frac{g}{3}}{\sqrt{1-\frac{2g}{3}}} < c < \sqrt{1-\frac{g}{3}}$. The plane is divided into C_{RN} , C_S and C_{AN} according to the stability of the critical manifold. The sets F_u (bounded) and F_s (unbounded) are the boundaries between C_{RN} and C_S , respectively, C_S and C_{AN} . There are four folded singularities f_1, \dots, f_4 for these values of c . Two of these, f_1 and f_2 , are indicated using two disks (blue and green) at $v = \pm \mathbf{v}_s$. The two blue circles indicate f_3 and f_4 which are saddles, with the blue curves being the stable manifolds. The red star is the regular singularity q at $v = \mathbf{c}$, which is a saddle located within C_S . The case $\sqrt{1-\frac{g}{3}} < c < v_s$ is similar, but the nonsymmetric folded singularities f_3 and f_4 are then located on the F_s -branch shown in the lower left corner.

partially hyperbolic, the linearization having one single nonzero eigenvalue given by $2g < 0$. The associated eigenvector is $(1, 1, 0, 0)$ i.e. along the “symmetric fast” space $v_1 = v_2$. In terms of the center manifold computations, it is therefore useful to introduce

$$x = \frac{1}{2}(v_1 + v_2), \quad u = \frac{1}{2}(v_1 - v_2), \quad (24)$$

so that $u = 0$ corresponds to $v_1 = v_2$ in which case we also have $x = v_1 = v_2$. At the same time, it is also convenient to define a similar change of

coordinates on the set of slow variables:

$$y = \frac{1}{2}(w_1 + w_2) - w_s, \quad z = \frac{1}{2}(w_1 - w_2), \quad (25)$$

recall also (12). This gives the following system:

$$\begin{aligned} \dot{x} &= -x^3 + 3x - (y - w_s) - 3xu^2, \\ \dot{u} &= -z - u^3 + 3(v_s^2 - x^2)u, \\ \dot{y} &= \epsilon(x - c), \\ \dot{z} &= \epsilon u, \end{aligned} \quad (26)$$

for which the symmetric subspace is now defined by $u = z = 0$. In particular, the equations are now symmetric with respect to

$$\mathcal{S} : (u, z) \mapsto (-u, -z), \quad (27)$$

leaving x and y fixed. The linearization of (26) around $(v_s, 0, w_s, 0)$ for $\epsilon = 0$ again leads to the nonzero eigenvalue $2g < 0$, but now (by construction) the associated eigenvector is aligned with the u -axis. At the same time, we find a three-dimensional center space spanned by the vectors

$$((2g)^{-1}, 0, 1, 0)^T, (0, 1, 0, 0)^T, (0, 0, 0, 1)^T.$$

By center manifold theory, we obtain the following result.

Proposition 2 *There exists an attracting four dimensional symmetric (with respect to \mathcal{S} , see (27)) center manifold M_a of the extended system ((26), $\dot{\epsilon} = 0$) near $(x, u, y, z, \epsilon) = (v_s, 0, 0, 0, 0)$. It is locally a graph over (u, y, z, ϵ) , i.e. there is a neighborhood N of $(u, y, z, \epsilon) = (0, 0, 0, 0)$ such that*

$$M_a : x = v_s + \frac{1}{2g}y + \frac{3}{2g}v_s u^2 + m(u, y, z, \epsilon), \quad (u, y, z, \epsilon) \in N, \quad (28)$$

where the function $m : N \rightarrow \mathbb{R}$ is smooth and invariant with respect to \mathcal{S} :

$$m(u, y, z, \epsilon) = m(-u, y, -z, \epsilon),$$

for all $(u, y, z, \epsilon) \in N$ (where the right-hand is defined), and satisfies:

$$m(u, y, z, \epsilon) := \mathcal{O}(\epsilon, uz, u^4, y^2, z^2). \quad \square$$

PROOF The existence of a (symmetric) center manifold follows from standard theory [7, 21]. The expansion (28) is also the result of a direct calculation. ■

2.4 The reduced dynamics on M_a

We now proceed to study the reduced dynamics on M_a . For this, we insert (28) into (26) and obtain

$$\begin{aligned}\dot{u} &= -z - \frac{1}{g} (3v_s y + (9v_s^2 + g)u^2 + n(u, y, z, \epsilon)) u, \\ \dot{y} &= \epsilon \left(v_s - c + \frac{1}{2g} y + \frac{3v_s}{2g} u^2 + m(u, y, z, \epsilon) \right), \\ \dot{z} &= \epsilon u,\end{aligned}\tag{29}$$

on M_a . Here we have introduced a new smooth function $n : N \rightarrow \mathbb{R}$ satisfying

$$n(u, y, z, \epsilon) = \mathcal{O}(\epsilon, uz, u^2 y, u^4, y^2, z^2).$$

The function n is also invariant with respect to \mathcal{S} : $n(u, y, z, \epsilon) = n(-u, y, -z, \epsilon)$ for all $(u, y, z, \epsilon) \in N$ (where the right-hand side is well-defined).

The system (29) is slow-fast with one fast variable u and two slow variables y and z . We first describe the layer problem associated with (29):

$$\begin{aligned}\dot{u} &= -z - \frac{1}{g} (3v_s y + (9v_s^2 + g)u^2 + n(u, y, z, 0)) u, \\ \dot{y} &= 0, \\ \dot{z} &= 0,\end{aligned}\tag{30}$$

We then have the following result.

Lemma 3 *The critical manifold S of (30) is locally a graph over u, y :*

$$S : \quad z = Q(u, y),\tag{31}$$

where

$$Q(u, y) = -\frac{u}{g} (3v_s y + (9v_s^2 + g)u^2 + \mathcal{O}(y^2, u^2 y, u^4)),$$

with $9v_s^2 + g = 9 - 5g > 0$, see (6). The function Q is smooth and odd in u : $Q(-u, y) = -Q(u, y)$ for all u, y sufficiently small. Moreover, locally S splits into a disjoint union $S_a \cup F \cup S_r$ where

$$S_{r,a} := S \cap \{y \geq f(u^2)\}, \quad F = S \cap \{y = f(u^2)\},\tag{32}$$

where

$$f(u^2) := -\frac{9v_s^2 + g}{v_s} u^2 + \mathcal{O}(u^4).\tag{33}$$

Finally, the point $(u, y, z) = (0, 0, 0)$ is a cusp singularity of S . \square

PROOF The result follows from the implicit function theorem. In particular, by implicit differentiation S is non-normally hyperbolic at points where $\frac{\partial Q}{\partial u}(u, y) = 0$; solving this equation, depending smoothly on y and u^2 , gives $y = f(u^2)$ with f as in (33), or

$$u^2 = f^{-1}(y) = -\frac{v_s}{9v_s^2 + g}y + \mathcal{O}(y^2), \quad (34)$$

locally by the implicit function theorem. Inserting (34) into $z = Q(u, y)$ gives

$$z^2 + ay^3[1 + \mathcal{O}(y)] = 0,$$

upon squaring both sides. Here $a = \frac{4v_s^3}{(9v_s^2 + g)g^2} > 0$. Setting $\bar{y} = y[1 + \mathcal{O}(y)]^{1/3}$ and $\bar{z} = z/\sqrt{a}$ finally gives the cusp normal form $\bar{z}^2 + \bar{y}^3 = 0$ [1]. ■

Notice that S is symmetric; $(u, y, z) \in S$ implies that $(-u, y, -z) \in S$ for all (u, y, z) sufficiently small. In particular, $(0, y, 0) \in S$ for all $y \approx 0$. We illustrate the situation in Fig. 11.

Any point $p \in W^s(S_a)$, belongs to the stable manifold of a base point on S_a . We shall denote this base point by

$$\pi_a(p) \in S_a, \quad (35)$$

see Fig. 11.

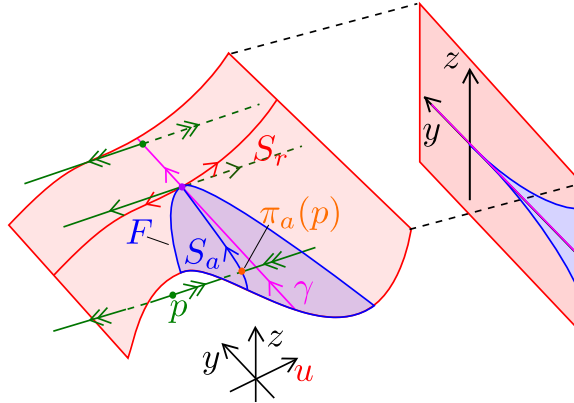


Figure 11: Sketch of the singular dynamics of (29) for $\epsilon = 0$ and $c \approx v_s(g)$ but $c < v_s(g)$, illustrating how the critical manifold splits into a repelling sheet S_r and an attracting sheet S_a along the degenerate set F , see also Lemma 3. The purple point indicates the cusp singularity (visible in the projection onto the (y, z) -plane), which acts like a node for the desingularized reduced problem on S_a . Due to the symmetry of the problem, the set γ (in pink) given by $u = z = 0$ is invariant for all $\epsilon > 0$.

Let

$$A(u, v) := \begin{pmatrix} 1 & -Q'_y(u, y) \\ 0 & Q'_u(u, y) \end{pmatrix}.$$

Here $Q'_s := \frac{\partial Q}{\partial s}$ denotes the partial derivative of Q with respect to $s = u, y$. Then the reduced problem on S can be written as

$$Q'_u(u, y) \begin{pmatrix} \dot{u} \\ \dot{y} \end{pmatrix} = A(u, v) \begin{pmatrix} u, \\ v_s - c + \frac{1}{2g}y + \frac{3}{2g}v_s u^2 + m(u, y, Q(u, y), 0), \end{pmatrix}, \quad (36)$$

by implicit differentiation.

Lemma 4 (36) is smoothly conjugated to the reduced problem (17) on C in a neighborhood of $v = \mathbf{v}_s$, $w = \mathbf{w}_s$. \square

PROOF This is by construction: The critical S within M_a is the set of equilibria of (26) and this set coincides with C upon application of the coordinate transformation defined by (24) and (25). We therefore obtain the desired transformation through the u -equation in (24) and the y -equation in (25):

$$u = \frac{1}{2}(v_1 - v_2), \quad y = \frac{1}{2}(h_1(v_1, v_2) + h_2(v_1, v_2)) - w_s. \quad (37)$$

We see that $v = \mathbf{v}_s$ gives $(u, y) = (0, 0)$ and the Jacobian matrix of the right hand sides with respect to $v = \mathbf{v}_s$ is

$$\begin{pmatrix} \frac{1}{2} & -\frac{1}{2} \\ g & g \end{pmatrix}.$$

Since this matrix is regular, having determinant $g < 0$, (37) defines a diffeomorphism $(v_1, v_2) \mapsto (u, y)$ on a neighborhood of $v = \mathbf{v}_s$ by the inverse function theorem and this gives the desired conjugacy between (36) and (17). \blacksquare

Consequently, our results on (17), see e.g. Proposition 1, can (locally) be transferred to (36). It will, however, be useful to perform the analysis of (36) in the u, y -plane directly nonetheless. To do so, we study a desingularization of (36). Specifically, since $Q'_u < 0$ on S_a , the system

$$\begin{pmatrix} \dot{u} \\ \dot{y} \end{pmatrix} = -A(u, v) \begin{pmatrix} u, \\ v_s - c + \frac{1}{2g}y + \frac{3}{2g}v_s u^2 + m(u, y, Q(u, y), 0), \end{pmatrix} \quad (38)$$

is equivalent to (36) there. Orbits of (36) on S_r are also orbits of the desingularized system (38) but the direction of the flow has changed. $(u, y) = (0, 0)$

is then an equilibrium of the desingularized system (38), and a direct calculation shows that the eigenvalues of the linearization are $(-2g)\lambda_1, (-2g)\lambda_2$, recall (23). Therefore for all c in the interval $\frac{1-\frac{g}{3}}{\sqrt{1-\frac{2g}{3}}} < c < v_s$, $(u, y) = (0, 0)$ is a hyperbolic stable node for (36), recall also Proposition 1. In particular, using (23) we find that $\lambda_1 = \lambda_2 < 0$ for $c = \frac{1-\frac{1}{2}g}{\sqrt{1-\frac{2g}{3}}}$. This value of c is always less than v_s for $g < 0$ (and greater than the value $\frac{1-\frac{1}{3}g}{\sqrt{1-\frac{2g}{3}}}$ corresponding to the second pitchfork bifurcation, recall Proposition 1). A direct calculation then gives the following.

Lemma 5 *Consider*

$$c \in \left(\frac{1 - \frac{1}{2}g}{\sqrt{1 - \frac{2g}{3}}}, v_s \right). \quad (39)$$

Then

$$\lambda_2 < \lambda_1 < 0, \quad (40)$$

and the invariant set $u = 0$ is therefore the weak direction of the stable node $(u, y) = (0, 0)$. \square

Consequently, all points on S_a approaches $(u, y) = (0, 0)$ tangentially to the set $u = 0$ under the forward flow of (38) for these values of c . In the following, we shall denote the corresponding set $(0, y, 0)$ in the (u, y, z) space by γ . For c as in (39), it corresponds to a singular weak canard for the folded node [53]. In fact, γ is distinguished from all orbits on S_a insofar that it is symmetric with respect to \mathcal{S} .

As S has a cusp singularity at $(u, y, z) = 0$, $v = \mathbf{v}_s, w = h(\mathbf{v}_s)$ is not a regular folded node singularity [53] of the slow-fast system (1). We refer to it as a **cusped node**.

Notice also that in the nonhyperbolic case $c = v_s$, it follows from $Q(0, y) = 0$ that the invariant set γ becomes an attracting center manifold of (38) along which we have $\dot{y} = \frac{3v_s}{2g}y^2(1 + \mathcal{O}(y)) > 0$ on S_a . Despite the resemblance, the transcritical bifurcation at $c = v_s$ is also not a folded saddle-node (type II) [31]. We will instead call it a **cusped saddle-node**.

In the following, we describe the dynamics of (29) near the cusped node $(u, y, z) = 0$ for $\epsilon = 0$ (corresponding to $v = \mathbf{v}_s$ in Fig. 10) for c -values fixed in the interval (39). Here we will blowup $(u, y, z, \epsilon) = 0$ and describe how trajectories that start near S_a will evolve as they pass the folded singularity. Subsequently, we will turn our attention to the cusped saddle-node. For this purpose, we will (essentially) include c in the blowup transformation and blowup $(u, y, z, \epsilon, c) = (0, 0, 0, 0, v_s)$. This will enable us to describe the onset and termination of MMOs.

Remark 2 The point $(u, y) = (0, 0)$ also has a strong eigendirection for (38) along $y = 0$ whenever (39) holds. In fact, a direct calculations shows that $\dot{u} < 0$ along the fold $y = f(u^2)$, $u \neq 0$, and, as a consequence, the strong stable manifold for (38) lies completely within the repelling subset S_r of S in this case, see the red orbit on S in Fig. 11. Therefore, since the direction is reversed on S_r , it follows that (36) does not have a strong canard (in contrast to the standard folded node).

The lack of a strong canard relates to another important difference between the folded node and the cusped node. Indeed, for the folded node, there is only one fast direction away from the fold. In contrast, as we see in Fig. 11, there are two separate fast directions (in green, using single headed arrows to indicate the lack of hyperbolicity) away from the cusp. \square

3 Blowup analysis of the cusped node

Consider the extended system obtained from augmenting (29) by $\dot{\epsilon} = 0$ for the parameter values (39) and denote the resulting right hand side by $V(u, y, z, \epsilon, c)$. Then $(u, y, z, \epsilon) = 0$ is a degenerate equilibrium of the vector-field V , with the linearization having only zero eigenvalues. We therefore perform a spherical blowup transformation [13, 46] of $(u, y, z, \epsilon) = 0$:

$$\Psi : (r, (\bar{u}, \bar{y}, \bar{z}, \bar{\epsilon})) \mapsto \begin{cases} u &= r\bar{u}, \\ y &= r^2\bar{y}, \\ z &= r^3\bar{z}, \\ \epsilon &= r^4\bar{\epsilon}, \end{cases} \quad (41)$$

with $r \in [0, r_0]$, $r_0 > 0$ small enough, $(\bar{u}, \bar{y}, \bar{z}, \bar{\epsilon}) \in S^3$ where

$$S^3 = \left\{ (x_1, x_2, x_3, x_4) \in \mathbb{R}^4 : \sum_{i=1}^4 x_i^2 = 1 \right\},$$

is the unit 3-sphere. In this way, the degenerate point $(u, y, z, \epsilon) = 0$ gets blown up through the preimage of (41) to the 3-sphere with $r = 0$. Let $\bar{V} = \Psi^*V$ denote the pull-back of V under (41). Then the exponents on r (also called weights) in (41) have been chosen so that

$$\widehat{V} := r^{-2}\bar{V}, \quad (42)$$

is well-defined and non-trivial for $r = 0$. \widehat{V} , being equivalent with V for $r > 0$, will have improved hyperbolicity properties for $r = 0$ and it is therefore this vector-field that we will study in the following. To do so we will use certain directional charts [30]. We will focus on two charts: the ‘‘entry chart’’ obtained by setting $\bar{y} = -1$ in (41), and the ‘‘scaling chart’’ obtained by setting $\bar{\epsilon} = 1$ in (41). That is, we consider local coordinates $(r_1, u_1, z_1, \epsilon_1)$

and (r_2, u_2, y_2, z_2) , parametrizing the subset of the sphere where $\bar{y} < 0$ and where $\bar{\epsilon} > 0$, respectively, such that (41) takes the following local forms:

$$(r_1, u_1, z_1, \epsilon_1) \mapsto \begin{cases} u &= r_1 u_1, \\ y &= -r_1^2, \\ z &= r_1^3 z_1, \\ \epsilon &= r_1^4 \epsilon_1. \end{cases} \quad (43)$$

and

$$(r_2, u_2, y_2, z_2) \mapsto \begin{cases} u &= r_2 u_2, \\ y &= r_2^2 y_2, \\ z &= r_2^3 z_2, \\ \epsilon &= r_2^4. \end{cases} \quad (44)$$

respectively. We will refer to these charts as $\bar{y} = -1$ and $\bar{\epsilon} = 1$ in the following and the dynamics in each of these are analyzed in the following sections. Notice that the charts (43) and (44) overlap on $\bar{y} < 0, \bar{\epsilon} > 0$ and the associated change of coordinates is given by the following expressions:

$$r_2 = r_1 \epsilon_1^{1/4}, \quad z_2 = z_1 \epsilon_1^{-3/4}, \quad y_2 = -\epsilon_1^{-1/2}, \quad u_2 = u_1 \epsilon_1^{-1/4}, \quad (45)$$

for $\epsilon_1 > 0$. In the following, we analyze the dynamics in each of the two charts. The analysis of the remaining charts, required to cover the sphere completely, is similar and therefore left out. We summarize our findings in Fig. 12. We refer to the figure caption for further details. In the following, we will use the convention that a set, say P , will be given a subscript 1 or 2 when expressed in the respective charts $\bar{y} = 1$ and $\bar{\epsilon} = 1$. When the charts overlap, P_1 will then be related by P_2 under the change of coordinates (45).

Remark 3 The references [5, 24] also describe a slow-fast cusp singularity in \mathbb{R}^3 using GSPT and blowup. However, their blowup weights differ from ours since these references consider the cusp in absence of singularities of the reduced flow. The results of [5, 24] therefore generalizes [47] on regular jump points. Moreover, at the level of the layer problem our setting corresponds to a time reversal of the system in [5, 24], i.e. their $S_{a,r}$ correspond to our $S_{r,a}$, respectively. \square

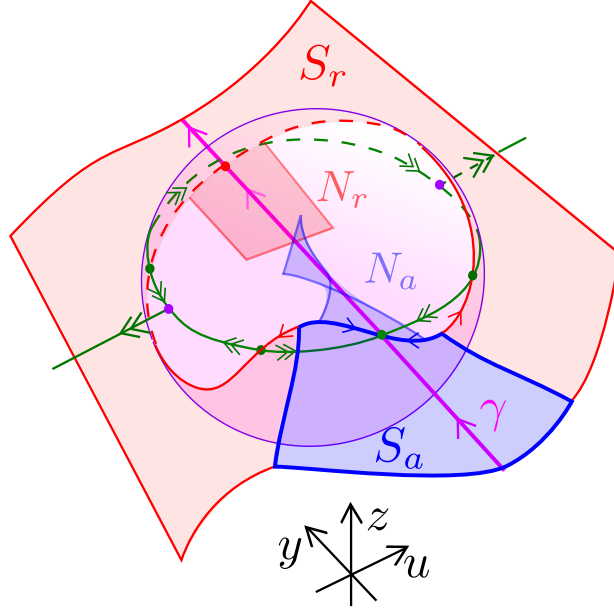


Figure 12: Illustration of the spherical blowup of the cusped node. The blowup transformation (41) allows us to extend subsets of the critical manifolds $S_{a,r}$ onto the sphere S^3 as invariant manifolds $N_{a,r}$ of a desingularized vector-field. Since $\bar{\epsilon} \geq 0$, we illustrate the resulting hemi-sphere as a solid sphere (shaded and purple) with $\bar{\epsilon} > 0$ inside. As indicated, these extended manifolds, which lie inside, intersect transversally along γ in general (when the ratio $\frac{\lambda_2}{\lambda_1}$ of the eigenvalues is not an integer, see Lemma 7) and the number of twists of N_a and N_r along γ can, as in the folded node, be directly related to the number of SAOs, see Theorem 2.

3.1 Analysis in the $\bar{y} = -1$ -chart

Inserting (43) into (29) with $\dot{\epsilon} = 0$ augmented gives

$$\begin{aligned}
\dot{r}_1 &= -\frac{1}{2}r_1\epsilon_1 \left[v_s - c + r_1^2 \left(-\frac{1}{2g} + \frac{3v_s}{2g}u_1^2 + \mathcal{O}(r_1^2) \right) \right], \\
\dot{u}_1 &= -z_1 - \frac{1}{g} \left(-3v_s + (9v_s^2 + g)u_1^2 + \mathcal{O}(r_1^2) \right) u_1 \\
&\quad + \frac{1}{2}u_1\epsilon_1 \left[v_s - c + r_1^2 \left(-\frac{1}{2g} + \frac{3v_s}{2g}u_1^2 + \mathcal{O}(r_1^2) \right) \right], \\
\dot{z}_1 &= \epsilon_1 \left(u_1 + \frac{3}{2}z_1 \left[v_s - c + r_1^2 \left(-\frac{1}{2g} + \frac{3v_s}{2g}u_1^2 + \mathcal{O}(r_1^2) \right) \right] \right), \\
\dot{\epsilon}_1 &= 2\epsilon_1^2 \left[v_s - c + r_1^2 \left(-\frac{1}{2g} + \frac{3v_s}{2g}u_1^2 + \mathcal{O}(r_1^2) \right) \right],
\end{aligned} \tag{46}$$

after division of the right hand side by r_1^2 . All \mathcal{O} -terms are smooth functions. This is our local form of \widehat{V} , recall (42). The set $r_1 = \epsilon_1 = 0$ is invariant and on this set we find that $\dot{z}_1 = 0$ and

$$\dot{u}_1 = -z_1 - \frac{1}{g} (-3v_s + (9v_s^2 + g)u_1^2) u_1.$$

There is therefore a critical manifold S_1 along $r_1 = \epsilon_1 = 0$ given by

$$z_1 = -\frac{1}{g} (-3v_s + (9v_s^2 + g)u_1^2) u_1. \quad (47)$$

It is the critical manifold S extended to the blowup sphere, where it has improved hyperbolicity properties. In particular, let

$$u_{p,1} := \sqrt{\frac{v_s}{9v_s^2 + g}}. \quad (48)$$

Then the subset $S_{a,1}$ of S_1 within $u_1 \in (-u_{p,1}, u_{p,1})$ is partially attracting, the linearization about any point in this set $(r_1, u_1, z_1, \epsilon_1) \in S_{a,1}$ having one single nonzero and negative eigenvalue. Consequently, by center manifold theory we obtain the following result.

Proposition 3 *For any $\nu > 0$ small enough, consider $I(\nu) := [-u_{p,1} + \nu, u_{p,1} - \nu]$. Then there exists a three dimensional center manifold $N_{a,1}$ of points $(0, u_1, 0, 0)$, $u_1 \in I(\nu)$ of the following graph form:*

$$N_{a,1} : \quad z_1 = u_1 \left(-\frac{1}{g} (-3v_s + (9v_s^2 + g)u_1^2) + \mathcal{O}(r_1^2, \epsilon_1) \right), \quad (49)$$

for $u_1 \in I(\nu)$, $(r_1, \epsilon_1) \in [0, \delta]^2$ and some $\delta > 0$ small enough. \square

In the expansion (49), we have used that $u_1 = z_1 = 0$ is invariant for all $r_1, \epsilon_1 \geq 0$.

As usual, $N_{a,1}$ is foliated by constant ϵ -values: $\epsilon = r_1^4 \epsilon_1$ and $N_{a,1} \cap \{\epsilon = r_1^4 \epsilon_1\}$ therefore provides an extension of Fenichel's slow manifold $S_{a,\epsilon}$, being a perturbation of a compact subset of S_a , up close to the blowup sphere. Specifically, at $\epsilon_1 = \delta$ we have $r_1 = \epsilon^{1/4} \delta^{-1/4} = \mathcal{O}(\epsilon^{1/4})$ and $N_{a,1} \cap \{\epsilon = r_1^4 \epsilon_1\}$, upon blowing down to the (u, y, z) -variables, therefore extends $S_{a,\epsilon}$ as an invariant manifold up to a "wedge-shaped" region of $(0, 0, 0)$ which extends $\mathcal{O}(\epsilon^{1/4})$, $\mathcal{O}(\epsilon^{1/2})$, $\mathcal{O}(\epsilon^{3/4})$ in the u, y, z -directions, respectively, recall (41).

A direct calculation shows that the reduced problem on $N_{a,1}$ is given by

$$\begin{aligned} \dot{r}_1 &= -\frac{1}{2} r_1, \\ \dot{u}_1 &= u_1 \left(-\frac{\lambda_2}{\lambda_1} + \frac{1}{2} + \mathcal{O}(u_1^2, r_1^2, \epsilon_1) \right), \\ \dot{\epsilon}_1 &= 2\epsilon_1, \end{aligned} \quad (50)$$

recall (23). Here we have used a desingularization through division by

$$\epsilon_1 [v_s - c + \mathcal{O}(r_1^2)];$$

notice that the square bracket is positive for any $r_1 \geq 0$ small enough by assumption of (39). Then for c as in (39), see also (40), one can show that $(r_1, u_1, \epsilon_1) = 0$ is the only equilibrium on $N_{a,1}$ and it is hyperbolic for (50) with eigenvalues

$$-\frac{1}{2}, -\frac{\lambda_2}{\lambda_1} + \frac{1}{2}, 2. \quad (51)$$

Lemma 6 *Suppose that (40) holds and that*

$$\frac{\lambda_2}{\lambda_1} \neq 3.$$

Then there is a C^1 -linearization of (50) of the form:

$$(r_1, u_1, \epsilon_1) \mapsto \tilde{u} = \psi(r_1, u_1, \epsilon_1), \quad (52)$$

where $\psi(0, 0, 0) = 0$, $\frac{\partial \psi}{\partial u_1}(0, 0, 0) = 1$, so that

$$\dot{\tilde{u}}_1 = \tilde{u}_1 \left(-\frac{\lambda_2}{\lambda_1} + \frac{1}{2} \right).$$

□

PROOF According to the classical work [4], a smooth system $\dot{x} = Ax + \mathcal{O}(x^2)$, with eigenvalues ν_i , $i = 1, \dots, n$, of the matrix $A \in \mathbb{R}^{n \times n}$, is linearizable by a C^1 -diffeomorphism if

$$\nu_i \neq \operatorname{Re}(\nu_j + \nu_k),$$

for all $i = 1, \dots, n$ and all $\operatorname{Re} \nu_j < 0$ and $\operatorname{Re} \nu_k > 0$. In the present case, this gives

$$-\frac{\lambda_2}{\lambda_1} + \frac{1}{2} \neq -\frac{1}{2} + 2 = \frac{3}{2},$$

setting $\nu_i = -\frac{\lambda_2}{\lambda_1} + \frac{1}{2}$, $\nu_j = -\frac{1}{2}$ and $\nu_k = 2$, and

$$-\frac{1}{2} \neq -\frac{\lambda_2}{\lambda_1} + \frac{1}{2} + 2 = -\frac{\lambda_2}{\lambda_1} + \frac{5}{2},$$

setting $\nu_i = -\frac{1}{2}$, $\nu_j = -\frac{\lambda_2}{\lambda_1} + \frac{1}{2}$, and $\nu_k = 2$, recall (51). The first inequality clearly holds since the left hand side is negative by (40). Similar, the second inequality implies $\lambda_2 \neq 3\lambda_1$ and the existence of the C^1 -linearization therefore follows. Seeing that the r_1 - and ϵ_1 -equations are already linear, one can easily show that the linearization takes the form (52). ■

3.2 Analysis in the $\bar{\epsilon} = 1$ -chart

Inserting (44) into (29) with $\dot{\epsilon} = 0$ augmented gives

$$\begin{aligned} \dot{u}_2 &= -z_2 - \frac{1}{g} (3v_s y_2 + (9v_s^2 + g)u_2^2 + \mathcal{O}(r_2^2)) u_2, \\ \dot{y}_2 &= v_s - c + r_2^2 \left(\frac{1}{2g} y_2 + \frac{3v_s}{2g} u_2^2 + \mathcal{O}(r_2^2) \right), \\ \dot{z}_2 &= u_2, \end{aligned} \tag{53}$$

and $\dot{r}_2 = 0$, upon division of the right hand side by the common factor r_2^2 . All \mathcal{O} -terms are smooth. This is our local form of \widehat{V} , recall (42). Notice that since $\gamma : u = z = 0$ is invariant for all $\epsilon \geq 0$, the set γ_2 defined by $u_2 = z_2 = 0$ is also invariant for all $r_2 \geq 0$ and y_2 increases for c in the interval (39) for all $0 < r_2 \ll 1$. Consider $r_2 = 0$. Then we obtain

$$\begin{aligned} \frac{du_2}{dy_2} &= \frac{1}{v_s - c} \left(-z_2 - \frac{1}{g} (3v_s y_2 + (9v_s^2 + g)u_2^2) u_2 \right), \\ \frac{dz_2}{dy_2} &= \frac{u_2}{v_s - c}. \end{aligned}$$

Linearization around $u_2 = z_2 = 0$ gives

$$\begin{aligned} \frac{dU_2}{dy_2} &= \frac{1}{v_s - c} \left(-Z_2 - \frac{3v_s}{g} y_2 U_2 \right), \\ \frac{dZ_2}{dy_2} &= \frac{U_2}{v_s - c}. \end{aligned} \tag{54}$$

Setting

$$y_2 = \sqrt{\frac{-g(v_s - c)}{3v_s}} Y_2,$$

we can write this system as a Weber equation:

$$U_2''(Y_2) - Y_2 U_2'(Y_2) + \frac{\lambda_2}{\lambda_1} U_2(Y_2) = 0, \tag{55}$$

recall (23). The implication of this is the following: Let $N_{a,2}(r_2)$ denote the center manifold obtained in the chart $\bar{y} = -1$ written in the $\bar{\epsilon} = 1$ -coordinates (u_2, y_2, z_2, r_2) . It is parametrized by $r_2 = \epsilon^{1/4}$ and $N_{a,2}(0)$ denotes the intersection with $r_2 = 0$, i.e. with the blowup sphere.

Working in the $\bar{y} = 1$ chart, for example, we may also obtain a repelling critical manifold $N_{2,r}(r_2)$ in much the same way. This extends the repelling slow manifold $S_{r,\epsilon}$ into scaling chart as an invariant manifold and we write $N_{2,r}(0)$ to denote the intersection with $r_2 = 0$. We extend each of these manifolds by the flow and denote the extended objects by the same symbol. Then $\gamma_2 \subset N_{a,2}(0) \cap N_{2,r}(0)$. Using (55), we have the following.

Lemma 7 *The intersection of $N_{a,2}(0)$ and $N_{2,r}(0)$ along γ_2 is transverse whenever $\frac{\lambda_2}{\lambda_1} \notin \mathbb{N}$. In the affirmative case, the tangent space of $N_{a,2}(0)$ along γ_2 twists $\lfloor \frac{\lambda_2}{\lambda_1} \rfloor$ -many times, where each twist corresponds to a full rotation by 180° degrees. \square*

PROOF The proof of this is identical to the proof of [46, Lemma 4.4] for the folded node. Basically, regarding the transversality, we first use that the tangent spaces of $N_{a,2}(0)$ and $N_{2,r}(0)$ along γ_2 coincide with the set of solutions of (54) having algebraic growth as $y_2 \rightarrow \mp\infty$, respectively. Next, for $\frac{\lambda_2}{\lambda_1} \notin \mathbb{N}$ it is standard that there are no bounded solutions of (55). This proves the transversality. Finally, regarding the number of twists, we use that any solution of (55) having algebraic growth as $y_2 \rightarrow -\infty$ has $\lfloor \frac{\lambda_2}{\lambda_1} \rfloor + 1$ simple zeros. Two consecutive zeros correspond to a full 180° -rotation in the (U_2, Z_2) -plane and the result therefore follows. \blacksquare

Remark 4 Whenever $n := \frac{\lambda_2}{\lambda_1} \in \mathbb{N}$, then $U_2(Y_2) = H_n(Y_2/\sqrt{2})$, with H_n the Hermite polynomial of degree n , is a bounded solution of (55), see [53]. This means that $TN_{a,2}(0) = TN_{r,2}(0)$ and the tangent spaces form a single band with $\frac{\lambda_2}{\lambda_1}$ -many twists. This may give rise to secondary intersections of $N_{a,2}$ and $N_{a,r}$ (like secondary canards, see [27, 53]) upon perturbation. But in contrast to the folded node, the bifurcations $\frac{\lambda_2}{\lambda_1} \in \mathbb{N}$ do not produce additional intersections of the Fenichel slow manifolds themselves, since in our case we do not have a strong canard, recall Remark 2. See also [27]. We therefore do not pursue the description of these bifurcations any further. \square

3.3 Completing the analysis of the cusped node

We can now state our main results on the dynamics for fixed c in the interval (39). Firstly, following Lemma 7 and the fact that $N_{a,2}(r_2)$ and $N_{2,r}(r_2)$ are $\mathcal{O}(r_2^2)$ -close to $N_{a,2}(0)$ and $N_{2,r}(0)$ in the scaling chart, we conclude:

Proposition 4 *The Fenichel slow manifolds $S_{a,\epsilon}$ and $S_{r,\epsilon}$ intersect transversally along γ whenever $\lfloor \frac{\lambda_2}{\lambda_1} \rfloor \notin \mathbb{N}$ for all $0 < \epsilon \ll 1$. \square*

Remark 5 A similar result holds for the folded node, see e.g. [46, 53]. But in contrast to these results, we are here deliberately referring to the Fenichel slow manifolds, i.e. the slow manifolds obtained from perturbing compact subsets of S_a and S_r through Fenichel's theory [15] and extending these by the forward flow. For the general folded node, it is only invariant manifolds – that have been extended as center-like manifolds – that are shown to intersect transversally along a weak canard; the Fenichel slow manifolds are only a subset of these extended manifolds. This relates to the delicacy of the weak canard and whether this object in fact ever reaches the Fenichel slow manifolds, see also [27] for a discussion of these technical aspects. The reason why we can be more specific in the present context is that γ , which

plays the role of the weak canard, exists for all $\epsilon > 0$ for our system and this set therefore (locally) belongs to $S_{a,\epsilon}$ and $S_{r,\epsilon}$. \square

We now proceed to state our main result on the SAOs of the cusped node. For this, we will follow [53] and count, in line with Lemma 7, the number of SAOs as the number of full 180° -rotations in a plane transverse to γ . More precisely, consider an orbit $O : t \mapsto (u(t), y(t), z(t))$, $t \in I := [0, T]$, with

$$(u(t), z(t)) \neq (0, 0),$$

for all $t \in I$. The number of SAOs is then the rotation number

$$n = \lfloor (\Theta(T) - \Theta(0)) / \pi \rfloor,$$

where $\Theta(t) \in \mathbb{R}$, $t \in [0, T]$, is the lift of the angle $\theta(t) \in \mathbb{R}/2\pi\mathbb{Z}$ defined by $\tan \phi(t) = \frac{z(t)}{u(t)}$, $t \in [0, T]$. Similarly, we define the amplitude of the SAOs as $\max_{t \in [0, T]} |(u(t), z(t))|$. (In Theorem 3, however, we will measure the amplitude in terms of $|(u_2(t), z_2(t))|$).

In the following, we write $f = f(\mu) \sim \mu$ whenever there are positive constants $c_1 < c_2$ such that

$$c_1 \mu \leq f(\mu) \leq c_2 \mu,$$

for all $0 < \mu \ll 1$.

Theorem 2 *Fix c as in (39), any $\delta > 0$ sufficiently small and suppose that*

$$\frac{\lambda_2}{\lambda_1} \notin \mathbb{N}.$$

Consider any point p so that $\pi_a(p) \in S_a \setminus \gamma$, recall (35). Then the following holds for all $0 < \epsilon \ll 1$: The forward orbit of p intersects the section defined by $y = y_{\text{exit}} := (\epsilon \delta^{-1})^{1/2}$ in a point $(u, y, z) = (u_{\text{exit}}, y_{\text{exit}}, z_{\text{exit}})$ with

$$u_{\text{exit}} \sim \epsilon^{\frac{\lambda_2}{2\lambda_1}}, \quad z_{\text{exit}} \sim \epsilon^{\frac{1}{2} + \frac{\lambda_2}{2\lambda_1}}, \quad (56)$$

and undergoes $\lfloor \frac{\lambda_2}{\lambda_1} \rfloor$ many SAOs. The order of the amplitude of the SAOs are given by (56). \square

PROOF We first work in the $\bar{y} = -1$ chart. Then the forward flow of the point p can be described by the reduced problem (50). We therefore integrate these equations from $(r_{10}, u_{10}, \epsilon_{10})$ to $(r_{11}, u_{11}, \epsilon_{11})$ with $\epsilon_{11} = \delta > 0$. Here $r_{10}, u_{10} = \mathcal{O}(1)$ and $\epsilon_{10} \sim \epsilon$ as $\epsilon \rightarrow 0$ by assumption on $\pi_a(p) \notin \gamma$. To perform the integration, we apply Lemma 6 and consider

$$\begin{aligned} \dot{r}_1 &= -\frac{1}{2}r_1, \\ \dot{\tilde{u}}_1 &= \tilde{u}_1 \left(-\frac{\lambda_2}{\lambda_1} + \frac{1}{2} \right), \\ \dot{\epsilon}_1 &= 2\epsilon_1. \end{aligned}$$

Integrating these equations gives

$$\tilde{u}_{11} = (\epsilon_{11}^{-1} \epsilon_{10})^{\frac{\lambda_2}{2\lambda_1} - \frac{1}{4}} \tilde{u}_{10},$$

and $r_{11} = (\epsilon \delta^{-1})^{1/4}$. Therefore $u_{11} \sim \epsilon^{\frac{\lambda_2}{2\lambda_1} - \frac{1}{4}}$ using (52). We then transform the result using (45) to the scaling chart. Here we apply regular perturbation theory from $y_2 = -\delta^{-1/3}$, which corresponds to $\epsilon_1 = \delta$, up to $y_2 = \delta^{-1/3}$. This value of y_2 corresponds to y_{exit} . Now, the order of the amplitude of u_2 and z_2 does not change during this finite time passage. Using (49) and (43), we therefore finally obtain (56). The number of small amplitude oscillations follow from Lemma 7 upon taking $\delta > 0$ small enough (and subsequently $\epsilon > 0$ small enough). \blacksquare

4 Analysis of the cusped saddle-node

Next, we consider the cusped saddle-node where $c \approx v_s$ in (29). For this we will use an ϵ -dependent zoom near v_s . Looking at (53) with $r_2 = \epsilon^{1/4}$, we see that

$$c = v_s + \sqrt{\epsilon} c_2, \tag{57}$$

brings the two terms in the equation for y_2 to the same order. For this reason, we now consider (57) before applying the blowup transformation Φ . In this way, $c = v_s$ gets blown up to $c_2 \in \mathbb{R}$ for $\epsilon = 0$. In the following, we study each of the charts $\bar{y} = -1$ and $\bar{\epsilon} = 1$ again. The results are summarized in Fig. 13.

4.1 Analysis in the $\bar{y} = -1$ -chart

The resulting equations can be obtained from (46) upon substituting (57). We have

$$\begin{aligned} \dot{r}_1 &= -\frac{1}{2} r_1^3 \epsilon_1 \left[-\sqrt{\epsilon_1} c_2 + \left(-\frac{1}{2g} + \frac{3v_s}{2g} u_1^2 + \mathcal{O}(r_1^2) \right) \right], \\ \dot{u}_1 &= -z_1 - \frac{1}{g} (-3v_s + (9v_s^2 + g)u_1^2 + \mathcal{O}(r_1^2)) u_1 \\ &\quad + \frac{1}{2} r_1^2 u_1 \epsilon_1 \left[-\sqrt{\epsilon_1} c_2 + \left(-\frac{1}{2g} + \frac{3v_s}{2g} u_1^2 + \mathcal{O}(r_1^2) \right) \right], \\ \dot{z}_1 &= \epsilon_1 \left(u_1 + \frac{3}{2} z_1 r_1^2 \left[-\sqrt{\epsilon_1} c_2 + \left(-\frac{1}{2g} + \frac{3v_s}{2g} u_1^2 + \mathcal{O}(r_1^2) \right) \right] \right), \\ \dot{\sqrt{\epsilon_1}} &= r_1^2 \epsilon_1 \sqrt{\epsilon_1} \left[-\sqrt{\epsilon_1} c_2 + \left(-\frac{1}{2g} + \frac{3v_s}{2g} u_1^2 + \mathcal{O}(r_1^2) \right) \right], \end{aligned}$$

writing the last equation in terms of $\sqrt{\epsilon_1}$ rather than ϵ_1 to indicate that the system is smooth in the former. For $r_1 = \sqrt{\epsilon_1} = 0$, we again find (47)

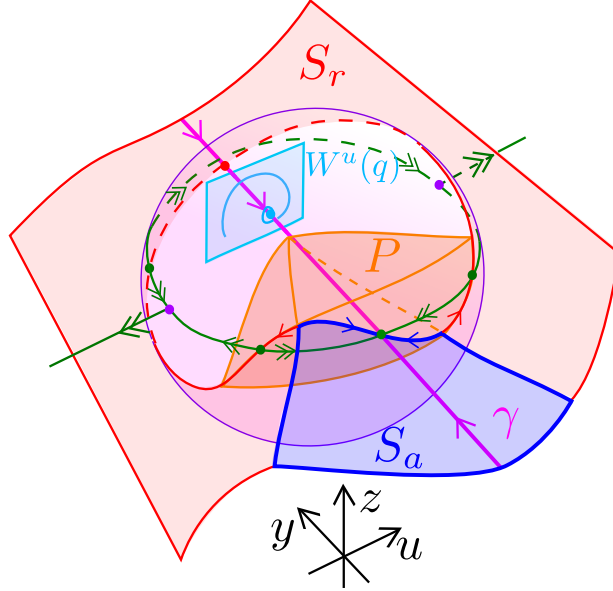


Figure 13: Illustration of the spherical blowup of the cusped saddle-node, using the same perspective as in Fig. 12. In this case, we obtain a slow-fast system on the blowup sphere with γ as a critical manifold. The reduced problem on γ has an equilibrium q which undergoes a Hopf bifurcation for the full system. In particular, on one side of the bifurcation q is of saddle-focus type (the cyan surface illustrates the unstable manifold $W^s(q)$) and this is where an increased number of SAOs occur. The fast subsystem of the slow-fast system on the blowup sphere is of Lienard-type and this gives rise to a cylinder P of limit cycles on the blowup sphere (in orange).

as a manifold of equilibria with the same stability properties. Therefore Proposition 3 still applies, but the remainder is now smooth in $\sqrt{\epsilon_1}$. The reduced problem is then

$$\begin{aligned}
 \dot{r}_1 &= -\frac{1}{2}r_1^3, \\
 \dot{u}_1 &= u_1 \left(-\frac{g^2}{3v_s} + \mathcal{O}(u_1^2, r_1^2, \sqrt{\epsilon_1}) \right), \\
 \dot{\sqrt{\epsilon_1}} &= r_1^2 \sqrt{\epsilon_1},
 \end{aligned} \tag{58}$$

after division of the right hand side by $\epsilon_1 \left[-\frac{1}{2g} + \mathcal{O}(r_1, \sqrt{\epsilon_1}) \right]$. Notice that the bracket is positive for all $r_1, \sqrt{\epsilon_1} \geq 0$ sufficiently small. From this we have.

Proposition 5 *Fix any c_2 with c as in (57), any $\delta > 0$ sufficient small and consider any point p so that $\pi_a(p) \in S_a \setminus \gamma$. Then the following holds for*

all $0 < \epsilon \ll 1$: The forward flow of p intersects the section defined by $y = y_{\text{in}} := -(\epsilon\delta^{-1})^{1/2}$ in a point $(u, y, z) = (u_{\text{in}}, y_{\text{in}}, z_{\text{in}})$ with

$$u_{\text{in}}, z_{\text{in}} = \mathcal{O}(e^{-\nu/\sqrt{\epsilon}}), \quad (59)$$

for some $\nu > 0$. □

PROOF We work in the entry chart $\bar{y} = -1$, reduce to $N_{a,1}$, divide (58) by \dot{r}_1 and integrate from $r_1 = \mathcal{O}(1)$ to $r_{1,\text{in}} = \mathcal{O}(\epsilon^{1/4})$ (corresponding to the value of $y = y_{\text{in}}$). This leads to the estimate

$$|u_{1,\text{in}}| \leq C e^\nu \int_{r_1}^{r_{1,\text{in}}} s^{-3} ds = C e^{\frac{1}{2}\nu r_1^{-2}} e^{-\frac{1}{2}\nu r_{1,\text{in}}^{-2}}$$

for some $C > 0$ and $\nu > 0$ independent of ϵ . ■

Next, we notice the following: Consider the $r_1 = 0$ subsystem:

$$\begin{aligned} \dot{u}_1 &= -z_1 - \frac{1}{g} (-3v_s + (9v_s^2 + g)u_1^2) u_1, \\ \dot{z}_1 &= \epsilon_1 u_1, \\ \dot{\epsilon}_1 &= 0. \end{aligned} \quad (60)$$

This system is a slow-fast Liénard system in the (u_1, z_1) -plane with $\epsilon_1 \geq 0$ as the small parameter. The analysis is straightforward and illustrated in Fig. 14. In particular, the associated layer problem has the set (47) as a manifold of equilibria, being attracting for $u_1 \in (-u_p, u_p)$ and repelling for $u_1 \notin [-u_{p,1}, u_{p,1}]$, recall (48). The reduced problem has a stable node at $(u_1, z_1) = 0$ on the attracting branch and we are therefore in the “relaxation regime”, but the relaxation oscillations for $\epsilon_1 > 0$ small enough are repelling. (Notice that in contrast to (2), the middle branch of the critical manifold of (60) is attracting. Compare also Fig. 1 with Fig. 14.) Therefore we have the following:

Lemma 8 *On $r_1 = 0$ there exists an invariant cylinder P_1 , contained within $\epsilon_1 \in [0, \delta]$, for $\delta > 0$ small enough, such that $P_1(\epsilon_{10}) := P_1 \cap \{\epsilon_1 = \epsilon_{10}\}$ is a repelling limit cycle for each $\epsilon_{10} \in (0, \delta]$. In particular, $P_1(0)$ is a singular slow-fast relaxation cycle.* □

4.2 Analysis in the $\bar{\epsilon} = 1$ -chart

The resulting equations can be obtained from (53) upon substituting (57). We have

$$\begin{aligned} \dot{u}_2 &= -z_2 - \frac{1}{g} (3v_s y_2 + (9v_s^2 + g)u_2^2 + \mathcal{O}(r_2^2)) u_2, \\ \dot{y}_2 &= r_2^2 \left(-c_2 + \frac{1}{2g} y_2 + \frac{3v_s}{2g} u_2^2 + \mathcal{O}(r_2^2) \right), \\ \dot{z}_2 &= u_2, \end{aligned} \quad (61)$$

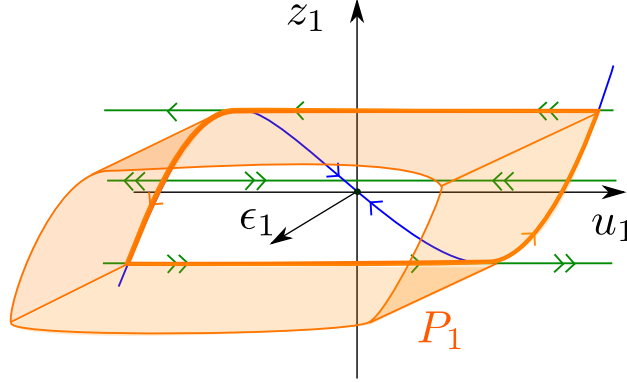


Figure 14: The invariant cylinder P_1 in the $\bar{y} = -1$ -chart within $r_1 = 0$. For $\epsilon_1 = 0$, it becomes a singular van der Pol-like relaxation cycle in the (u_1, z_1) -plane.

and $\dot{r}_2 = 0$. This is now a slow-fast system with two fast variables, u_2 and z_2 , and one single slow variable y_2 . In particular, we notice that

$$\gamma_2 : \quad u_2 = z_2 = 0, \quad y_2 \in \mathbb{R},$$

is now a critical manifold for $r_2 = 0$. In fact, the associated fast sub-system

$$\begin{aligned} \dot{u}_2 &= -z_2 - \frac{1}{g} (3v_s y_2 + (9v_s^2 + g)u_2^2) u_2, \\ \dot{z}_2 &= u_2, \end{aligned} \tag{62}$$

with y_2 fixed as a parameter for $r_2 = 0$, is a Lienard equation.

Lemma 9 *The system (62) has a unique repelling limit cycle $P_2(y_2)$ for each $y_2 < 0$.* \square

PROOF This follows from Lienard's theorem [40]. In fact, (62) is topologically equivalent with the van-der Pol system in backward time. In particular, there is a subcritical Hopf bifurcation of (62) at $y_2 = 0$. \blacksquare

By uniqueness, the set P_2 coincides with P_1 upon using the change of coordinates (45) where these overlap.

By Fenichel's theory [15], the manifold P_2 of repelling limit cycles of (61) for $r_2 = 0$, perturbs as an invariant manifold P_{2,r_2} within compact subsets. It creates a funnel region, where trajectories inside contract towards γ_2 , while trajectories outside get repelled away from the local neighborhood of the cusp. On the perturbed cylinder, repelling limit cycles may exist. This depends upon c_2 . Indeed, the reduced problem on P_2 is given by averaging:

Let $T(y_2)$ be the period of $P_2(y_2)$ as a periodic orbit $(u_2(t; y_2), z_2(t; y_2))$ of (62). Then

$$y_2' = -c_2 + \frac{1}{2g}y_2 + \frac{3v_s}{2g} \frac{1}{T(y_2)} \int_0^{T(y_2)} u_2(t; y_2)^2 dt, \quad (63)$$

on P_2 . Consequently, the reduced problem has an equilibrium at y_2 for the parameter value c_2 whenever

$$c_2 = \frac{1}{2g}y_2 + \frac{3v_s}{2g} \frac{1}{T(y_2)} \int_0^{T(y_2)} u_2(t; y_2)^2 dt, \quad y_2 < 0. \quad (64)$$

Notice that $y_2 = 0$ on the right hand side gives $c_2 = 0$. It is possible to show that $u(t, y_2) = 2\sqrt{\frac{-y_2 v_s}{9v_s^2 + g}} \cos(t) + \mathcal{O}(y_2)$ (using e.g. a Melnikov computation, see [28], where a similar computation is performed in a related context). This gives a linear approximation of the right hand side of (64):

$$c_2 \approx \frac{3v_s^2 + g}{2g(9v_s^2 + g)} y_2. \quad (65)$$

Consequently, the right hand side is a decreasing function of y_2 for $y_2 < 0$ small enough for $g < 0$. Numerical computations (see Fig. 15) indicate that this holds for all $y_2 < 0$. We have not found a way to show this, but if we assume this, then we have the following result.

Proposition 6 *Suppose that the right hand side of (64) is a strictly decreasing function of $y_2 < 0$. Fix any $c_{20} > 0$ and let y_{20} be the unique value y_2 such that (64) holds with $c_2 = c_{20}$. Then the reduced problem (63) on P_2 has a unique attracting fixed point at $y_2 = y_{20}$ for the parameter value $c_2 = c_{20}$.*

Moreover, for all $0 < r_2 \ll 1$, the corresponding singular cycle $P_2(y_{20})$ then perturbs to a hyperbolic (saddle-type) limit cycle $P_{2,r_2}(y_{20})$ of (61) for $c_2 = c_{20}$. This limit cycle is $\mathcal{O}(r_2^2)$ -close to $P_2(y_{20})$. \square

As c_2 ranges over a compact subset I of $(0, \infty)$, we then obtain a family of repelling limit cycles on P_{2,r_2} for all $0 < \epsilon \leq \epsilon_0(I)$. Recall that $r_2 = \epsilon^{1/4}$. It is possible to show that the family P_{2,r_2} overlaps with the repelling Hopf cycles emanating from $y_2 = 0$ at $c_2 = 0$, recall Remark 6.

Remark 6 The Liapunov coefficient l_1 (recall (7)) of the Hopf bifurcation for $c_2 = 0$ (corresponding to $c = v_s(g)$) can be calculated from (61). Indeed, a direction calculation shows that the two-dimensional center manifold at the Hopf-point takes the following form

$$y_2 \approx -\frac{3v_s}{2} u_2^2 - \frac{3v_s}{2} z_2^2,$$

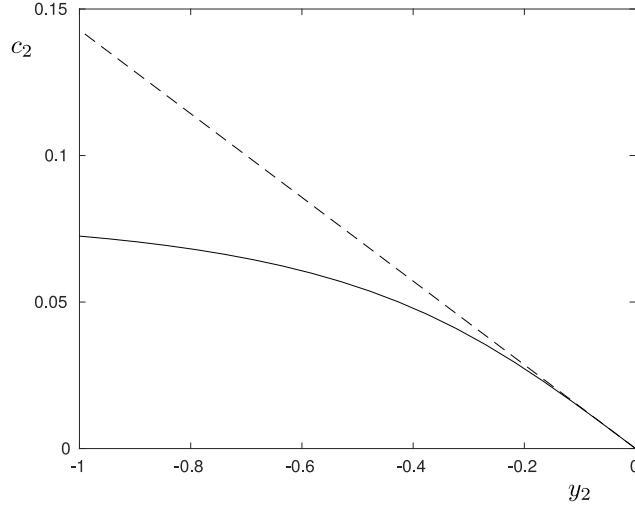


Figure 15: The right hand side of (64) as a function of y_2 for $g = -1$. The dotted line is the linear approximation (65) obtained through Melnikov. In order to compute the full line, we have first computed an accurate approximation of a limit cycle of (62) (using shooting and Newton's method) and then subsequently computed the average.

for $c_2, r_2 \rightarrow 0$, up to and including quadratic order in (u_2, z_2) . On this center manifold, with $c_2, r_2 \rightarrow 0$, we then have that

$$\begin{aligned} \dot{u}_2 &= -z_2 + f(u_2, z_2), \\ \dot{z}_2 &= u_2, \end{aligned} \tag{66}$$

with

$$f(u_2, z_2) \approx -\frac{1}{g} \left(-\frac{9}{2} v_s^2 z_2^2 + \left(\frac{9}{2} v_s^2 + g \right) u_2^2 \right) u_2,$$

up to an including cubic order in (u_2, z_2) . The system (66) is already in normal form and we therefore have that

$$\hat{l}_1 := \frac{1}{16} \left(\frac{\partial^3 f}{\partial u_2^3}(0,0) + \frac{\partial^3 f}{\partial u_2 \partial z_2^2}(0,0) \right) = \frac{3(g-3)}{8g}$$

using [19, Equation 3.4.11]. This gives the leading order expression in (7) upon division by $r_2^2 = \sqrt{\epsilon}$. This division corresponds to the desingularization in the chart $\bar{\epsilon} = 1$, recall (42). \square

We now proceed to study the properties of the critical manifold

$$\gamma_2 : \quad u_2 = z_2 = 0, y_2 \in \mathbb{R},$$

of (61) for $r_2 = 0$. The linearization of (62) around $u_2 = z_2 = 0$ gives

$$\begin{pmatrix} -\frac{3v_s}{g}y_2 & -1 \\ 1 & 0 \end{pmatrix}. \quad (67)$$

The eigenvalues are imaginary $\pm i$ for $y_2 = 0$ due to the Hopf. From this we can easily deduce the stability properties.

Lemma 10 *The critical manifold γ_2 of (61) for $r_2 = 0$ is normally hyperbolic for $y_2 \neq 0$. The subset γ_2^a with $y_2 < 0$ is attracting whereas the subset γ_2^r with $y_2 > 0$ is repelling. Moreover, $\gamma_2^r = \gamma_2^{rf} \cup \gamma_2^{rn}$ where γ_2^{rf} is the subset of γ_2 with $y_2 \in \left(0, -\frac{2g}{3v_s}\right)$ having normal focus stability (i.e. the eigenvalues of (67) are complex conjugated with positive real part) whereas γ_2^{rn} is the subset of γ_2^r with $y_2 \geq -\frac{2g}{3v_s}$ having normal nodal stability (i.e. the eigenvalues of (67) are real and positive). \square*

There is a similar division of $\gamma_2^a = \gamma_2^{af} \cup \gamma_2^{an}$ for $y_2 \in \left(\frac{2g}{3v_s}, 0\right)$ and $y_2 \leq \frac{2g}{3v_s}$, respectively, but this will be less important.

The reduced problem on γ_2 is given by

$$y_2' = -c_2 + \frac{1}{2g}y_2.$$

It has a hyperbolic and attracting equilibrium at $y_2 = 2c_2g$. In combination with Lemma 10, we realize the following.

Lemma 11 *Let q_2 denote the equilibrium $(u_2, y_2, z_2) = (0, 2c_2g, 0)$ which is hyperbolic and attracting for the reduced problem on γ_2 . Then the following holds.*

- For $c_2 > 0$, then q_2 sits on the attracting part of γ_2 and it perturbs to an attracting equilibrium (61) for all $0 < \epsilon \ll 1$.
- For $c_2 \in \left(-\frac{1}{3v_s}, 0\right)$, then $q_2 \in \gamma_2^{rf}$ and it perturbs to a saddle-focus equilibrium of (61) for all $0 < \epsilon \ll 1$ with a one-dimensional stable manifold along γ_2 and a two-dimensional unstable manifold with focus-type dynamics.
- For $c_2 < -\frac{1}{3v_s}$, then $q_2 \in \gamma_2^{rn}$ and it perturbs to a saddle equilibrium of (61) for all $0 < \epsilon \ll 1$ with a one-dimensional stable manifold along γ_2 and a two-dimensional unstable manifold with nodal-type dynamics. \square

We illustrate the findings in the $\bar{\epsilon} = 1$ -chart in Fig. 16. See figure caption for further details. We are now ready to describe our main result on small amplitude oscillations for the cusped saddle-node.

Theorem 3 Consider c as in (57) with $c_2 \in \left(-\frac{1}{3v_s}, 0\right)$ fixed and any point p so that $\pi_a(p) \in S_a \setminus \gamma$. Then the following holds for all $0 < \epsilon \ll 1$: The forward orbit of p intersects the section defined by $y = 0$ in a point $(u, y, z) = (u_0, 0, z_0)$ with

$$u_0, z_0 = \mathcal{O}(e^{-c/\sqrt{\epsilon}}). \quad (68)$$

The number of SAOs of the forward orbit is unbounded as $\epsilon \rightarrow 0$, but finitely many are $\mathcal{O}(1)$ in amplitude in the (u_2, z_2) -plane. \square

PROOF For $c_2 \in \left(-\frac{1}{3v_s}, 0\right)$, q_2 belongs to γ_2^{rf} and is of saddle-focus type, recall Lemma 11. (68) follows directly from the exponential contraction $e^{-c\tau/\sqrt{\epsilon}}$ towards the invariant γ_2^a on the slow time scale τ of (61); recall that $r_2 = \epsilon^{1/4}$. Due to the focus behavior of γ_2 near $y_2 = 0$, recall Lemma 10, the forward orbit will experience an unbounded number of SAOs as $\epsilon \rightarrow 0$. These will be exponentially small in amplitude. Moreover, since $\pi_a(p) \in S_a \setminus \gamma$ and γ_2 is the stable manifold of q_2 , the forward orbit of p will extend along γ_2^{rf} , remaining exponential close for all $y_2 \in [0, y_{21}(c_2)]$, for some $0 < y_{21}(c_2) < 2c_2g$. Beyond this, the orbit will eventually be repelled away from γ_2 due to the unstable manifold of q_2 . Since $q_2 \in \gamma_2^{rf}$ for $c_2 \in \left(-\frac{1}{3v_s}, 0\right)$, we obtain finitely many $\mathcal{O}(1)$ SAOs due to the focus dynamics in the (u_2, z_2) -projection at some distance from q_2 . This completes the proof. \blacksquare

Remark 7 With the assumptions of Theorem 3, there is a bifurcation delay along γ_2 . For the statement of the theorem, we did not need to determine this delay in details. However, due to the invariance of γ_2 , it can be determined by a way-in/way-out function in the following way: Let

$$\nu_{\pm}(y_2) = -\frac{3v_s}{2g}y_2 \pm \frac{1}{2}\sqrt{\frac{9v_s^2}{4g^2}y_2^2 - 4}, \quad (69)$$

denote the eigenvalues of (67). Then for $c_2 < 0$ the exit point $y_{2,\text{exit}} \in (0, 2c_2g)$ is for $r_2 \rightarrow 0$ determined by

$$\int_{-\infty}^{y_{2,\text{exit}}} \frac{\text{Re } \nu_+(y_2)}{-c_2 + \frac{1}{2g}y_2} dy_2 = 0. \quad (70)$$

(The integral is convergent since $\frac{\text{Re } \nu_+(y_2)}{-c_2 + \frac{1}{2g}y_2} \approx \frac{-4g^2}{3v_s y_2^2}$ for $y_2 \rightarrow -\infty$ and $y_{2,\text{exit}} > 0$ exists and is unique for each $c_2 < 0$ since $\frac{\text{Re } \nu_+(y_2)}{-c_2 + \frac{1}{2g}y_2} \rightarrow \infty$ for $y_2 \rightarrow 2c_2g^-$. $y_{2,\text{exit}}(c_2)$ is also continuous and $y_{2,\text{exit}}(0^-) = 0$.) The integral gives a lengthy expression and we have not found a way to solve for $y_{2,\text{exit}}$. We therefore only present a diagram (obtained in Matlab) for $g = -1$, see Fig. 17 and the figure caption for further details, of $y_{2,\text{exit}}$ as a function of c_2 .

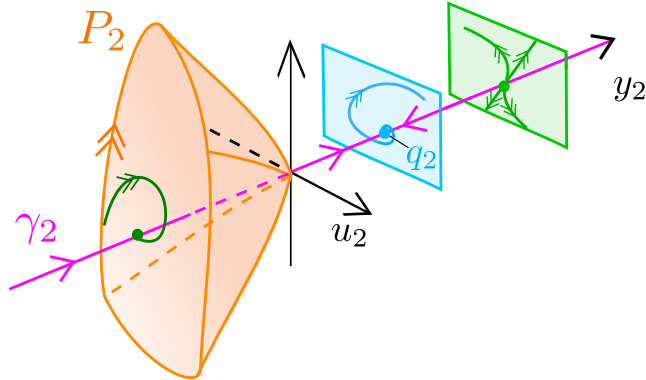


Figure 16: Illustration of the dynamics in the $\bar{e} = 1$ -chart in the case of the cusped saddle-node. The manifold of limit cycles P_2 is in orange while the critical manifold γ_2 is in pink. On the positive side of $y_2 = 0$, we illustrate the normal dynamics on γ_2^{rf} in cyan (focus type) and on γ_2^{rf} in green (nodal type). When the equilibrium $q_2 \in \gamma_2$ (also cyan) lies on γ_2^{rf} , SAOs of order $\mathcal{O}(1)$ (in the (u_2, y_2, z_2) -scaling) occur near $W^u(q_2)$.

Due the invariance of γ_2 , the delay for our system (1) is different from the bifurcation delay for the folded saddle-node, see e.g. [31]. Indeed, for the folded saddle-node, the delay for *analytic systems* depends upon (following [36, 37]) buffer points. If we were to break the symmetry of (1), then one would like to rely on the same methods. But this could be problematic in this context, since the center manifold in Proposition 2 is not expected to be analytic. \square

A similar result holds for $c_2 < -\frac{1}{3v_s}$, but due to the normal nodal dynamics along γ^{rn} all SAOs may be exponentially small in this case. We see this in Fig. 17 for the value of $g = -1$. In particular, for $c_2 < -0.42$ the exit point (green part of curve) is in the normal nodal regime where there are no additional $\mathcal{O}(1)$ -oscillations when the trajectory separate from γ_2 . For $c_2 > 0$, on the other hand, the forward flow of p is attracted to the stable equilibrium near q_2 .

Remark 8 Formally, the scaling (57) does not overlap with the regime covered by Theorem 2 where c is fixed in a compact subset of $c < v_s$. There is therefore a gap that we do not cover in this paper. However, to cover this gap, and obtain a complete description of c in a full neighborhood of v_s , one could include c in the blowup transformation (41) as follows

$$c = v_s + r^2 \bar{c},$$

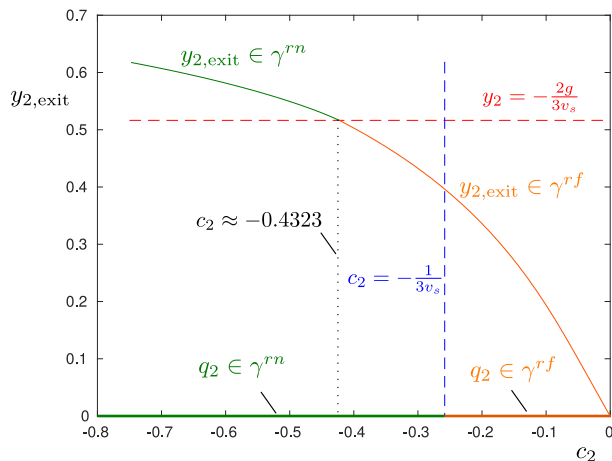


Figure 17: The graph of $y_{2,\text{exit}}(c_2)$ obtained from the equation (70) with $g = -1$ (in orange and in green). The blue line is $c_2 = -\frac{1}{3v_s}$, i.e. the value of c_2 such that q_2 is an improper node of the fast sub-system (62) (i.e. $\nu_- = \nu_+$, see (69)). The red line is the corresponding y_2 -value of q_2 : $y_2 = -\frac{2g}{3v_s}$. There is an intersection of the graph of $y_{2,\text{exit}}(c_2)$ with $y_2 = -\frac{2g}{3v_s}$ at $c_2 \approx -0.42$. This intersection divides the graph into two parts, indicated in orange and green where $(0, y_{2,\text{exit}}, 0) \in \gamma_2^{rf}$ and $(0, y_{2,\text{exit}}, 0) \in \gamma_2^{rn}$, respectively. (In the figure, we have abused notation slightly and written this more compactly as $y_{2,\text{exit}} \in \gamma_2^{rf}$ and $y_{2,\text{exit}} \in \gamma_2^{rn}$.)

and consider $(\bar{u}, \bar{y}, \bar{z}, \bar{e}, \bar{c}) \in S^4$. In particular, in this way, one could cover the gap by working in the directional chart corresponding to $\bar{c} = -1$. Notice that the associated scaling chart $\bar{e} = 1$ gives rise to the same coordinates $(u_2, y_2, z_2, r_2, c_2)$ where $c = v_s + r^2 c_2$ in agreement with (57). (This also motivates the use of the subscript on c , recall the convention before Remark 3.)

We shall not pursue this further in the present paper. \square

5 Conclusions

In this paper, we have analyzed cusped singularities (cusped node and cusped saddle-node) and demonstrated that they form a mechanism for SAOs in two coupled FitzHugh-Nagumo units with symmetric and repulsive coupling. As for the folded node, we showed that the number of SAOs is determined by the Weber equation and the ratio of eigenvalues of the cusped node (upon desingularization). Similarly, we showed that the cusped saddle-node marks the onset of SAOs. Although there are many similarities between the folded singularities and the cusped versions studied in the present paper, there are also several differences, see e.g. Remark 2 and

Lemma 9. Perhaps most importantly, our cusped node does not have a strong canard and there are also two fast directions away from the cusp (u increasing and u decreasing in Fig. 8), as opposed to just one in the case of the standard folded singularity. The latter property also has consequences on MMOs and the LAOs that we see in Fig. 2. For the folded node, MMOs occur if there is return to the funnel region, see [6]. The same is true in the present case, but it is slightly more subtle. Suppose (for definiteness) that there is a return mechanism to $S_a \setminus \gamma$, leaving the cusp region along the positive u -direction. Then as a consequence of Theorem 2, we obtain the following: Let $\lfloor \frac{\lambda_2}{\lambda_1} \rfloor$ be even (odd) and suppose that the return to S_a is on the u -positive side (u -negative side, respectively) of γ . Then we have (“one-sided”) MMOs for all $0 < \epsilon \ll 1$ with u always increasing upon passage through the cusp. However, if affirmative, then the system (1) – due to the symmetry \mathcal{S} – also has MMOs with u always decreasing upon passage through the cusp. In fact, more generally, once we have a return to $S_a \setminus \gamma$ along one direction (u -positive or u -negative), then the symmetry give rise to a return along the other direction (u -negative or u -positive, respectively) too. We can then also have (“mixed”) MMOs where u alternates sign upon passing through the cusp f_1 . We see this in Fig. 2 for $c = 1.27$. Indeed, here there is an alternation between v_1 and v_2 being increasing (v_2 , respectively, v_1 decreasing) which precisely corresponds to a change in sign in u . The description of the return mechanism for (1), and whether we have “one-sided” or “mixed” MMOs, require a careful analysis of the layer problem (13) but also of the reduced problem (14) (away from the cusp). We leave such an analysis to future work.

In future work, it would also be interesting to study the cusped singularities in a general setting without a symmetry. We already have some partial results in this direction. The cusped node then becomes a co-dimension one bifurcation of a folded node that transverses the cusp upon parameter variation. In line with our findings, the number of SAOs does not change upon this passage. Within this context, it would also be interesting in future work to study the secondary canards and the role of a strong canard.

Similarly, the cusped saddle-node becomes co-dimension two without the symmetry. However, going from a folded saddle-node to a cusped saddle-node seems slightly more involved. A folded saddle-node (type II) is accompanied by a canard-like explosion of limit cycles (due to the strong canard), see also [28]. In our symmetric cusped saddle-node there is no explosion, but instead a cylinder on which limit cycles occur, recall Proposition 6. It is unclear how this scenario unfolds without the symmetry and how it precisely connects to the folded saddle-node. Moreover, a folded saddle-node actually comes in two versions. We have only focused on type II in this manuscript [30], but there is also a type I [50]. Future research should also uncover how the generalized cusped saddle-node relates to these.

Acknowledgment

The authors are thankful for the discussions they have had with Morten Brøns in preparation of this manuscript.

References

- [1] V. I. ARNOLD, *Catastrophe Theory*, Springer Berlin Heidelberg, 1984.
- [2] K. BAR-ELI, *On the stability of coupled chemical oscillators*, Physica D, 14 (1985), pp. 242–252.
- [3] S. BATTAGLIN AND M. G. PEDERSEN, *Geometric analysis of mixed-mode oscillations in a model of electrical activity in human beta-cells*, Nonlinear Dynamics, 104 (2021), pp. 4445–4457.
- [4] G. R. BELITSKII, *Functional equations and conjugacy of local diffeomorphisms of a finite smoothness class*, Functional Analysis and Its Applications, 4 (1973), pp. 268–277, <https://doi.org/10.2307/2374346>.
- [5] H. W. BROER, T. J. KAPER, AND M. KRUPA, *Geometric desingularization of a cusp singularity in slow-fast systems with applications to Zeeman’s examples*, Journal of Dynamics and Differential Equations, 25 (2013), pp. 925–958, <https://doi.org/10.1007/s10884-013-9322-5>.
- [6] M. BRØNS, M. KRUPA, AND M. WECHSELBERGER, *Mixed mode oscillations due to the generalized canard phenomenon*, Fields Inst. Commun., 49 (2006), pp. 39–63.
- [7] J. CARR, *Applications of centre manifold theory*, vol. 35, New York: Springer-Verlag, 1981.
- [8] R. CURTU, *Singular Hopf bifurcations and mixed-mode oscillations in a two-cell inhibitory neural network*, Physica D: Nonlinear Phenomena, 239 (2010), pp. 504–514.
- [9] R. CURTU, AND J. RUBIN, *Interaction of canard and singular Hopf mechanisms in a neural model*, SIAM Journal on Applied Dynamical Systems, 10 (2011), pp. 1443–1479.
- [10] G. DE VRIES AND A. SHERMAN, *Channel sharing in pancreatic beta-cells revisited: enhancement of emergent bursting by noise*, J Theor Biol, 207 (2000), pp. 513–30, <https://doi.org/10.1006/jtbi.2000.2193>.

- [11] M. DESROCHES, J. GUCKENHEIMER, B. KRAUSKOPF, C. KUEHN, H. M. OSINGA, AND M. WECHSELBERGER, *Mixed-mode oscillations with multiple time scales*, SIAM Review, 54 (2012), pp. 211–288, <https://doi.org/10.1137/100791233>.
- [12] C. T. DICKSON, J. MAGISTRETTI, M. H. SHALINSKY, E. FRANSÉN, M. E. HASSELMO, AND A. ALONSO, *Properties and role of $I(h)$ in the pacing of subthreshold oscillations in entorhinal cortex layer II neurons*, J Neurophysiol, 83 (2000), pp. 2562–79, <https://doi.org/10.1152/jn.2000.83.5.2562>.
- [13] F. DUMORTIER AND R. ROUSSARIE, *Canard cycles and center manifolds*, Memoirs of the American Mathematical Society, 121 (1996), pp. 1–96.
- [14] G. ERMENTROUT AND N. KOPELL, *Oscillator death in systems of coupled neural oscillators*, SIAM J Appl Math, 50 (1990), pp. 125–146.
- [15] N. FENICHEL, *Geometric singular perturbation theory for ordinary differential equations*, J. Diff. Eq., 31 (1979), pp. 53–98.
- [16] R. FITZHUGH, *Impulses and physiological states in theoretical models of nerve membrane*, Biophys J, 1 (1961), pp. 445–466, [https://doi.org/10.1016/s0006-3495\(61\)86902-6](https://doi.org/10.1016/s0006-3495(61)86902-6).
- [17] T. GREGOR, K. FUJIMOTO, N. MASAKI, AND S. SAWAI, *The onset of collective behavior in social amoebae*, Science, 328 (2010), pp. 1021–5, <https://doi.org/10.1126/science.1183415>.
- [18] J. GUCKENHEIMER, *Singular Hopf bifurcation in systems with two slow variables*, SIAM Journal on Applied Dynamical Systems, 7 (2008), pp. 1355–1377.
- [19] J. GUCKENHEIMER AND P. HOLMES, *Nonlinear Oscillations, Dynamical Systems and Bifurcations of Vector Fields*, Springer, 1997.
- [20] Y. GUTFREUND, Y. YAROM, AND I. SEGEV, *Subthreshold oscillations and resonant frequency in guinea-pig cortical neurons: physiology and modelling*, J Physiol, 483 (Pt 3) (1995), pp. 621–40, <https://doi.org/10.1113/jphysiol.1995.sp020611>.
- [21] M. HARAGUS AND G. IOOSS, *Local Bifurcations, Center Manifolds, and Normal Forms in Infinite-Dimensional Dynamical Systems*, EDP Sciences, 2011.
- [22] A. L. HODGKIN AND A. F. HUXLEY, *A quantitative description of membrane current and its application to conduction and excitation in nerve*, J Physiol, 117 (1952), pp. 500–44.

- [23] E. M. IZHIKEVICH, *Dynamical systems in neuroscience*, MIT press, 2007.
- [24] H. JARDÓN-KOJAKHMETOV, H. W. BROER, AND R. ROUSSARIE, *Analysis of a slow-fast system near a cusp singularity*, Journal of Differential Equations, 260 (2016), pp. 3785–3843, <https://doi.org/10.1016/j.jde.2015.10.045>.
- [25] C. JONES, *Geometric Singular Perturbation Theory, Lecture Notes in Mathematics, Dynamical Systems (Montecatini Terme)*, Springer, Berlin, 1995.
- [26] J. KIMREY, T. VO, AND R. BERTRAM, *Big ducks in the heart: Canard analysis can explain large early afterdepolarizations in cardiomyocytes*, SIAM Journal on Applied Dynamical Systems, 19 (2020), pp. 1701–1735.
- [27] K. U. KRISTIANSEN, *On the pitchfork bifurcation of the folded node and other unbounded time-reversible connection problems in \mathbb{R}^3* , SIAM Journal on Applied Dynamical Systems, 19 (2020), pp. 2059–2102, <https://doi.org/10.1137/20M1326180>.
- [28] K. U. KRISTIANSEN, *The dud canard: Existence of strong canard cycles in \mathbb{R}^3* , arXiv:2207.00875v2 preprint, (2022).
- [29] M. KRUPA, B. AMBROSIO, AND M. AZIZ-ALAOUI, *Weakly coupled two-slow-two-fast systems, folded singularities and mixed mode oscillations*, Nonlinearity, 27 (2014), p. 1555.
- [30] M. KRUPA AND P. SZMOLYAN, *Extending geometric singular perturbation theory to nonhyperbolic points - fold and canard points in two dimensions*, SIAM Journal on Mathematical Analysis, 33 (2001), pp. 286–314, <http://epubs.siam.org/doi/abs/10.1137/S0036141099360919> (accessed 2014-06-02).
- [31] M. KRUPA AND M. WECHSELBERGER, *Local analysis near a folded saddle-node singularity*, Journal of Differential Equations, 248 (2010), pp. 2841–2888, <https://doi.org/10.1016/j.jde.2010.02.006>.
- [32] C. R. LAING, AND C. CARSON, *A spiking neuron model for binocular rivalry*, Journal of Computational Neuroscience, 12 (2002), pp. 39–53.
- [33] A. LOPPINI, M. BRAUN, S. FILIPPI, AND M. G. PEDERSEN, *Mathematical modeling of gap junction coupling and electrical activity in human β -cells*, Phys Biol, 12 (2015), p. 066002, <https://doi.org/10.1088/1478-3975/12/6/066002>.

- [34] A. LOPPINI AND M. G. PEDERSEN, *Gap-junction coupling can prolong beta-cell burst period by an order of magnitude via phantom bursting*, *Chaos*, 28 (2018), p. 063111, <https://doi.org/10.1063/1.5022217>.
- [35] J. NAGUMO, S. ARIMOTO, AND S. YOSHIZAWA, *An active pulse transmission line simulating nerve axon*, *Proceedings of the IRE*, 50 (1962), pp. 2061–2070.
- [36] A. NEISHTADT, *Persistence of stability loss for dynamical bifurcations .1*, *Differential Equations*, 23 (1987), pp. 1385–1391.
- [37] A. NEISHTADT, *Persistence of stability loss for dynamical bifurcations .2*, *Differential Equations*, 24 (1988), pp. 171–176.
- [38] M. G. PEDERSEN, *A comment on noise enhanced bursting in pancreatic beta-cells*, *J Theor Biol*, 235 (2005), pp. 1–3, <https://doi.org/10.1016/j.jtbi.2005.01.025>.
- [39] M. G. PEDERSEN, M. BRØNS, AND M. P. SØRENSEN, *Amplitude-modulated spiking as a novel route to bursting: Coupling-induced mixed-mode oscillations by symmetry breaking*, *Chaos*, 32 (2022), p. 013121, <https://doi.org/10.1063/5.0072497>.
- [40] L. PERKO, *Differential equations and dynamical systems*, Springer, 2001.
- [41] M. RIZ, M. BRAUN, AND M. G. PEDERSEN, *Mathematical modeling of heterogeneous electrophysiological responses in human β -cells*, *PLoS Comput Biol*, 10 (2014), p. e1003389, <https://doi.org/10.1371/journal.pcbi.1003389>.
- [42] H. G. ROTSTEIN, T. OPPERMAN, J. A. WHITE, AND N. KOPELL, *The dynamic structure underlying subthreshold oscillatory activity and the onset of spikes in a model of medial entorhinal cortex stellate cells*, *J Comput Neurosci*, 21 (2006), pp. 271–92, <https://doi.org/10.1007/s10827-006-8096-8>.
- [43] J. RUBIN AND M. WECHSELBERGER, *Giant squid-hidden canard: the 3D geometry of the Hodgkin-Huxley model*, *Biol Cybern*, 97 (2007), pp. 5–32, <https://doi.org/10.1007/s00422-007-0153-5>.
- [44] A. SHERMAN, *Anti-phase, asymmetric and aperiodic oscillations in excitable cells—I. Coupled bursters*, *Bull Math Biol*, 56 (1994), pp. 811–35.
- [45] A. SHERMAN AND J. RINZEL, *Rhythmogenic effects of weak electrotonic coupling in neuronal models*, *Proc Natl Acad Sci U S A*, 89 (1992), pp. 2471–4.

- [46] P. SZMOLYAN AND M. WECHSELBERGER, *Canards in \mathbb{R}^3* , J. Diff. Eq., 177 (2001), pp. 419–453, <https://doi.org/10.1006/jdeq.2001.4001>, <http://linkinghub.elsevier.com/retrieve/pii/S002203960194001X> (accessed 2014-05-26).
- [47] P. SZMOLYAN AND M. WECHSELBERGER, *Relaxation oscillation in \mathbb{R}^3* , Journal of Differential Equations, 200 (2004), pp. 69–104, <https://doi.org/10.1016/j.jde.2003.09.010>.
- [48] J. TABAK, N. TOPORIKOVA, M. E. FREEMAN, AND R. BERTRAM, *Low dose of dopamine may stimulate prolactin secretion by increasing fast potassium currents*, J Comput Neurosci, 22 (2007), pp. 211–22, <https://doi.org/10.1007/s10827-006-0008-4>.
- [49] T. VO, R. BERTRAM, J. TABAK, AND M. WECHSELBERGER, *Mixed mode oscillations as a mechanism for pseudo-plateau bursting*, J Comput Neurosci, 28 (2010), pp. 443–58, <https://doi.org/10.1007/s10827-010-0226-7>.
- [50] T. VO AND M. WECHSELBERGER, *Canards of folded saddle-node type I*, SIAM Journal on Mathematical Analysis, 47 (2015), pp. 3235–3283.
- [51] X.-J. WANG, AND J. RINZEL, *Alternating and synchronous rhythms in reciprocally inhibitory model neurons*, Neural Computation, 4 (1992), pp. 84–97.
- [52] A. WEBER, Y. PROKAZOV, W. ZUSCHRATTER, AND M. J. B. HAUSER, *Desynchronisation of glycolytic oscillations in yeast cell populations*, PLoS One, 7 (2012), p. e43276, <https://doi.org/10.1371/journal.pone.0043276>.
- [53] M. WECHSELBERGER, *Existence and bifurcation of canards in \mathbb{R}^3 in the case of a folded node*, SIAM Journal on Applied Dynamical Systems, 4 (2005), pp. 101–139, <https://doi.org/10.1137/030601995>, <http://epubs.siam.org/doi/abs/10.1137/030601995> (accessed 2014-05-26).
- [54] L. YARU AND L. SHENQUAN, *Characterizing mixed-mode oscillations shaped by canard and bifurcation structure in a three-dimensional cardiac cell model*, Nonlinear Dynamics, (2021), pp. 1–22, <https://doi.org/10.1007/s11071-021-06255-z>.